KWAME NKRUMAH UNIVERSITY OF SCIENCE AND TECHNOLOGY

COLLEGE OF ENGINEERING

Convergence Analysis of Massive MIMO Antenna Arrays Using a Geometry-Based Stochastic Channel Model

By

Patrick Danuor

(B.Sc. Telecommunications Engineering)

A Thesis submitted to the

Department of Telecommunications Engineering

College of Engineering

in partial fulfillment of the requirements for the degree of

MPHIL. TELECOMMUNICATIONS ENGINEERING

October 30, 2019

Declaration

I hereby declare that this thesis presented for the degree of Mphil. Telecommunications Engineering, is a presentation of my original work and to the best of my knowledge has not been submitted for any other degree or qualification. I confirm that appropriate credit has been given within this thesis where references have been made to the work of others.

Patrick Danuor	.....	.....
Student	Signature	Date

Certified by:

Dr. Emmanuel Ampoma Affum	.....	.....
Supervisor	Signature	Date

Certified by:

Ing. Dr. Abdul-Rahman Ahmed	.....	.....
Head of Department	Signature	Date

Dedication

This work is dedicated to God Almighty for His grace given me throughout this postgraduate studies, to my family and also to my colleagues.

Acknowledgement

Foremost, I would like to acknowledge the Almighty God for all my endeavors including putting this thesis together.

I would also like to express my sincere gratitude to my supervisor, Dr. Emmanuel Ampoma Affum, for the continuous support during my studies and research. His guidance, motivation and immense knowledge were very instrumental.

Finally, I must express my profound gratitude to my family for providing me with unfailing support throughout my years of study.

Abstract

In order to reap the full benefits of massive MIMO, the Base Station (BS) antennas must be significantly large to converge to favorable propagation condition or attain convergence (the state where the effect of noise and fast fading vanishes). However, increasing BS antennas results in closely spaced antenna elements which inadvertently leads to the detrimental effects of Spatial Correlation (SC) and that can affect the convergence of Massive MIMO System. So far, research works on Convergence have been investigated using Correlation-based Stochastic (CBSCM) channel models, which does not reflect accurate massive MIMO channel. This channel model does not take into consideration channel parameters such as the Pathloss, power delay profile as well as the characteristics of the antenna array needed for the practical massive MIMO system implementation. Therefore analysis of massive MIMO convergence regarding the Geometry-Based Stochastic Channel model (GBSCM), which reflects real practical massive MIMO channel and the effects of SC is needed. In this thesis, the convergence of massive MIMO based on GBSCM is studied. The effect of 3D SC of uniform rectangular and cylindrical array (URA and CA) based on the Maximum Power of Arrival (MPA) is incorporated. In the analysis, the Diagonal Dominance and Mean Absolute Deviation convergence metrics, were considered to study the effects of the SC on the asymptotic behavior of the channel matrix. The results support existing development that, increase in azimuth and elevation spreads of the angular distributions of arrival and antenna element spacing reduces the SC and thereby increases convergence rate of massive MIMO. Results also show poor performance for the Laplacian and Von Misses distributions in GBSCM, even for higher AS and ES, and angular spreads. Further it was realized that, in GBSCM, the convergence of massive MIMO was sensitive to antenna array topology regarding Gaussian and Student's t-distributions. This contradicts previously established results that convergence is insensitive to antenna topology in CBSCM.

List of Abbreviations (Acronymns)

2D	Two-dimensional
3D	Three-dimensional
3GPP	Third Generation Partnership Project
4G	Fourth Generation
5G	Fifth Generation
AoA	Azimuth Angle of Arrival
AoD	Azimuth Angle of Departure
AS	Azimuth Spread
AWGN	Additive White Gaussian Noise
BS	Base Station
CA	Cylindrical Array
CBSCM	Correlation-based Stochastic Channel Model
DD	Diagonal Dominance
DS	Delay Spread
EoA	Elevation Angle of Arrival
EoD	Elevation Angle of Departure
ES	Elevation Spread
FP	Favorable Propagation
GBSCM	Geometry-based Stochastic Channel Model
i.i.d.	Independently and identically distributed
LTE	Long Term Evolution
MAD	Mean Absolute Deviation
MPA	Maximum Power of Arrival
MAD	Mean Absolute Deviation
MC	Mutual Coupling
MIMO	Multiple-Input Multiple-Output
MS	Mobile Station

PL	Pathloss
RX	Receiver
SC	Spatial Correlation
SF	Shadow Fading
SNR	Signal-to-noise-Ratio
TDD	Time Division Duplex
TX	Transmitter
UCA	Uniform Circular Array
UE	User Equipment
ULA	Uniform Linear Array
URA	Uniform Rectangular Array
WINNER	Wireless World Initiative New Radio

Notation and Symbols

θ	Elevation Angle
ϕ	Azimuth Angle
θ_n	Elevation Angle of Departure
ϕ_n	Azimuth Angle of Departure
ϑ_n	Elevation Angle of Arrival
φ_n	Azimuth Angle of Arrival
ϕ_{tilt}	Elevation Angle of Antenna Boresight
μ	Measure of angular spread
κ	Accumulation of distribution
σ	Standard deviation
α	Decay Factor
λ	Eigenvalues
α_n	Complex Random Amplitude
$\mathbf{H}$	Channel Matrix
$\mathbf{E}$	Deviation Matrix
$\mathbf{W}$	Wishart Matrix
$\odot$	Hadamard Product
$\otimes$	Kronecker Product
$H_{i.i.d}$	Channel matrix with i.i.d. entries
$(.)^*$	Inverse of Matrix
$(.)^T$	Transpose of Matrix
$(.)^H$	Conjugate transpose of Matrix / Hermitian Matrix
$\|.\|$	Magnitude of Matrix
$\mathcal{CN}(\mu, \sigma^2)$	Complex normal distribution with mean μ and variance σ^2.
g_t	Gain of transmitter antenna
g_r	Gain of receiver antenna
$J_\alpha(.)$	Bessel function of the first kind

r	Cell radius
a_t	Array response of transmitter antenna
a_r	Array response of receiver antenna
π	Mathematical constant pi
$diag(.)$	Diagonal Matrix Elements
$det(.)$	Determinant of a Matrix
$Exp(.)$	Exponential Function
$\mathbf{v}$	Noise Vector
$\mathbf{x}$	Prerecord data vector
y	Received signal
$\mathbf{Z}$	Mutual Coupling Matrix
ξ	Shadow Fading
ζ	Angle of Arrival
ρ	Transmit Signal to noise Ratio
R_t	Transmit Spatial Correlation
R_r	Receiver Spatial Correlation
G	Channel Matrix
M	Number of Antennas
D_β	Diagonal Matrix

Contents

List of Tables

List of Figures

Chapter 1

Introduction

1.1 Research Background and Significance

1.1.1 Fifth Generation and Massive MIMO Technology

Multiple-input multiple-output (MIMO) is a novel method that utilizes multiple transmitters and receivers to send more information to users [1–3]. This technology has become increasingly popular among researchers in the wireless communications industry. This is because MIMO technology offers several benefits such as enhanced spectrum efficiency and improved network throughput [3,4]. This technology, also known as the multi-antenna system, finds its origins in antenna diversity, whose history dates back as far back in the 1920s [1]. In recent years, the MIMO technology has become popular due to its major achievements such as reduction in bit error rate, higher throughput as well as higher quality of service [5–8].

The underlying concept of the multi-antenna system technology is the principle of channel diversity, where the receiver is provided with various versions of the same transmitted signal in order to stabilize the channel as a result of the unstable wireless fading channel [9]. This technique improves the MIMO channel capacity and minimizes degradation in the bit error rate [10]. In urban environments, where the possibility of achieving line-of-sight is challenging, and the issue of interference due to abundance RF/microwave system is mostly high, MIMO technology has proven to be an ideal and efficient solution for communication to provide the bandwidth requirements that recent audio, data system, and video require. The robustness of MIMO techniques against channel fading and interference makes it strong to minimize the effect of lost or dropped data packets as

well as enabling high data rates [8]. Recently, studies have shown that transmitting multiple signals employing MIMO techniques in the same frequency channel increases spectral efficiency. [11,12]. In contrast to traditional single-input single-output schemes, other studies also show that the capacity of the MIMO system with n_{TX} and n_{RX} transmitting and receiving antennas respectively, can scale linearly by the factor of $min(n_{TX}, n_{RX})$ without utilizing extra transmitting power and channel bandwidth [5, 12, 13]. Foschini in [6] demonstrated this and generalized the upper bound channel capacity for the multi-antenna system in b/s /Hz as shown in equation (1.1),

$$C_{MIMO} = log_2[det(\mathbf{I} + \frac{SNR}{n_{TX}}\mathbf{H}.\mathbf{H}^H)] \tag{1.1}$$

where the channel matrix is denoted by $\mathbf{H}$ and the transmitted signal is composed of n_{TX} statistically independent equal power components each with a Gaussian distribution. $\mathbf{I}$ is defined as the $n_{TX} \times n_{RX}$ identity matrix and $\mathbf{H}^H$ is the Hermitian matrix. The important clarification of equation (1.1) is that in a multi-antenna system, the channel capacity can be enhanced by an increase in the number of transmitting and receiving antennas, or more precisely, by increasing the number of uncorrelated sub-channels [14]. Research conducted in this area shows that the MIMO system capability can possibly scale linearly with the minimum transmit (TX) and receive (RX) antennas for channel matrices with independent and identically distributed (i.i.d) components [5, 13]. Initially, these systems were intended to support antenna configurations that can only adapt in the azimuth. The future generation of mobile communications standards such as 3GPP and LTE-Advanced is aimed at supporting even greater data rate transmissions, which has stirred increasing interest among researchers in improving system efficiency through the use of adaptive electronic beam control over both azimuth and elevation dimensions [15]. The important effect of elevation on system performance has already been proved by several measurement campaigns [15]. The reason for this can be ascribed to its capacity to allow various strategies such as

user-specific elevation beamforming and 3D cell splitting.

To cope with the unprecedented growth and projected exponential increase in volume of wireless data traffic in the near future, there has been significant amount of research for the development of a potential next generation wireless system technology [15–18]. This has brought about the development of the fifth Generation (5G) wireless system. The 5G wireless system technology is expected to include an aggregate of data-rate increase, from Fourth Generation (4G) wireless systems, of three orders of magnitude with peak data rates in the order of tens of Gbps [19]. Seamless connectivity as well as very low latency has also been earmarked as one of the benefits of the 5G wireless system [20].

The 5G technology includes key requirements such as massive connectivity, ultra low latency and high data rates. This has prompted candidate technologies to be proposed and investigated and among these proposed technologies are the massive MIMO and small cell technology [18–20]. Massive MIMO, also known as large-scale antenna systems, technology is a novel and paradigm shift, envisioned to achieve significant wireless system enhancements for 5G [21–23], combined with improvements in area spectral efficiency, using small cell technology [24, 25]. The fundamental idea of employing massive MIMO is to take advantage of all the advantages of the conventional MIMO, but on a much more larger scale. Massive MIMO uses antenna arrays with approximately hundred antennas to simultaneously serve many dozen user terminals in the same time and frequency resource [22].

1.1.2 Antenna Arrays and Spatial Correlation

Antenna arrays are becoming progressively significant in the design of wireless communication networks principally because of its use in the exploitation of spatial properties to enhance MIMO channel capacity and large diversity [26]. One benefit of antenna array is the ability to change its radiation pattern in response to different excitation of its elements (both current phases and current magni-

tudes) [26]. This offers the opportunity to achieve a specific array pattern from the antenna array without altering the physical properties of the array. They can also provide diversity gain in the multipath reception [21].

With the deployment of the massive MIMO technology, various antenna array topologies have been proposed. Among them is the one-dimensional Uniform Linear Array (ULA), where the antenna array elements are arranged along a straight line as illustrated in Figure 1.1. The Uniform Circular Array (UCA) is illustrated in Figure 1.2. In the planar arrays, the position of the antenna elements lies in the xy-plane [26], or the position of the antenna elements are indicated by two variables representing polar or Cartesian coordinates such as the Uniform Rectangular Array (URA) and the Cylindrical Array (CA) shown in Figures 1.3 and 1.4, respectively. In Figure 1.5 the antenna elements of the URA lie in the azimuth and the zenith domains (zy-plane). This represents the large-scale form of the URA for future MIMO communications [21].The physical position of the elements must, in many instances, conform to the shape and the curved surface on which they are mounted. Examples of these are arrays mounted on aircraft, missiles, or submarines. These are referred to as non-planar arrays or conformal arrays [27]. The most commonly used geometries are the CA shown in Figure 1.4 and the URA shown in Figures 1.3 and 1.4 [26].

Both CA and URA antenna topologies are considered in this study.

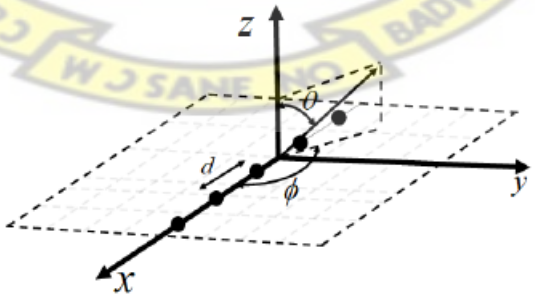

Figure 1.1: Geometry of the ULA, where d is the separation between the antenna elements, θ and ϕ are the elevation and the azimuth angles, respectively.

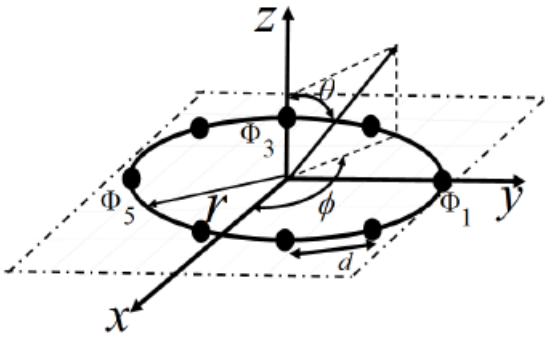

Figure 1.2: Geometry of the UCA, where r denotes the radius of the antenna array and $\Phi_s = 2\pi(s-1)/N$ defines the angular position of the s elements.

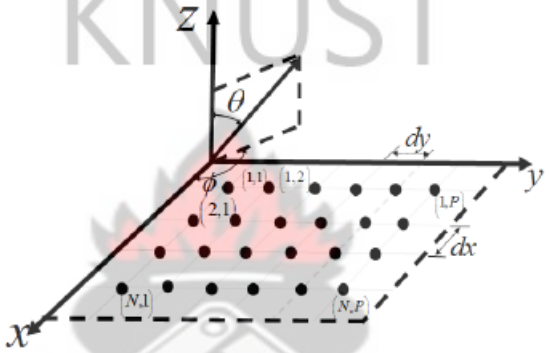

Figure 1.3: Geometry of the URA, where the antenna elements are parallel to the x and y-axis, (i.e. azimuth and elevation)

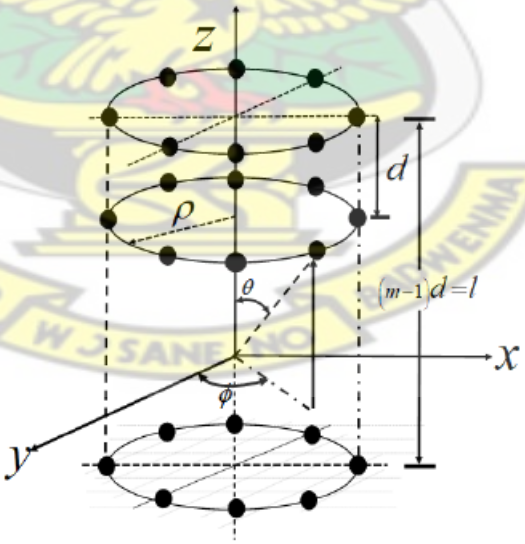

Figure 1.4: Geometry of the CA, ρ is the radius of the cylinder, where $d_z$wavelengths is the distance between the first and the second UCA in the z direction.

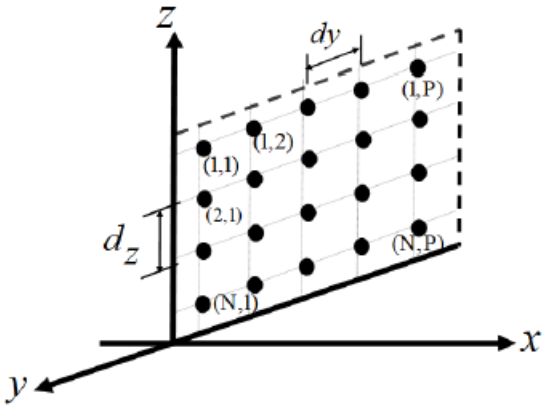

Figure 1.5: Geometry of the URA where the antenna elements are parallel to the azimuth and the zenith domains.

The antenna array configuration directly affects the channel characteristics which enhances the efficiency of massive MIMO [27]. The objective of massive MIMO is to employ as many antennas at the BS to exploit the channel's multi-path through diversity [22], as this is achieved by using large antenna arrays. However, with an increasing antenna elements in a close physical space to achieve higher transmission rate, a considerable amount of diversity results in two main effects. These include the spatial correlation (SC) and the mutual coupling (MC). The SC is as a result of the closeness of antenna elements as signal sources while the MC is as a result of the closeness of antenna elements as electrical components [28]. SC and MC reduces the multiplexing gains of massive MIMO thereby reducing the performance [29]. In order to prevent the detrimental effects of spatial correlation, antenna element separation of more than half wavelength is required [29, 30].

1.1.3 Favorable Propagation and Convergence

Further motivating the increase in research of massive MIMO systems are the additional beneficial channel properties which arise when operating with large numbers of transmitter antennas (TX). These properties arise as a result of random matrix theory asymptotics [31].

Considering an uplink of a single-cell system where K represents single-antenna

user terminals and M represent antennas at the BS. If the K terminals simultaneously transmit the K symbols $x_1, ..., x_K$, where $E[|x_k|^2] = 1$, then received vector at the BS is given by

$$\mathbf{y} = \sqrt{\rho}\mathbf{G}\mathbf{x} + \mathbf{w} \tag{1.2}$$

where $\mathbf{x} = [x_1, ..., x_K]^T$, $\mathbf{G} = [g_1, ..., g_K]$, $\mathbf{g}_k \in \mathcal{C}^{Mx1}$ is the channel vector between the BS and kth terminal, and the noise vector is defined as $\mathbf{w}$. ρ is the transmit signal to noise ratio (SNR). The channel vector $\mathbf{g}_k$ models the effects of large-scale fading and small-scale fading. The channel matrix, $\mathbf{G}$ is defined by,

$$\mathbf{G} = \mathbf{H}\mathbf{D}_{\beta}^{\frac{1}{2}} \tag{1.3}$$

where $\mathbf{H}$ is the $M \times K$ matrix which models the small-scale Rayleigh fading and spatial correlation, and $\mathbf{D}_{\beta}$ is a diagonal matrix modeling large-scale effects.

As the number of antennas at the BS becomes significantly large, (i.e. M $\rightarrow \infty$), the channel vectors between the *kth* terminal and the BS become mutually orthogonal, thereby canceling the effect of noise and large scale fading [23]. This condition is known as favorable propagation [32].

Favorable propagation is defined as the mutual orthogonality among the vector-valued channels to the terminals. It is one of the main characteristics of the radio channel used in massive MIMO [32]. Another salutary effect of using a large number of antennas at the BS eliminates the effects of uncorrelated receiver noise and fast fading [23]. The transmissions from terminals within one's own cell do not also interfere [23]. Random components also tend to be deterministic and matrix computations can be done much easier [23]. Linear processing methods can also attain optimum efficiency, with a simple linear detector like the matched filter, more explicitly on the uplink [26].

For favorable propagation to occur, the channel vectors $\mathbf{g}_k$, $k = 1, ..., K$, should be pair-wisely orthogonal. To be precise, the channel offers *favorable propagation*

if

$$\mathbf{g}_i^H \mathbf{g}_j = \begin{cases} 0, & i,j = 1,...,K, i \neq j \\ ||\mathbf{g}_k||^2 \neq 0 & k = 1,...,K. \end{cases} \tag{1.4}$$

In practice, equation (1.4) will never be satisfied exactly, but it can be approximately achieved [32]. In this case, the channel is said to offer *approximately* favorable propagation [32]. Also, considering some assumptions of the propagation environment, when M grows large and $k \neq j$, it holds that

$$\frac{1}{M}\mathbf{g}_k^H \mathbf{g}_j \to 0, M \to \infty \tag{1.5}$$

For this case, the channel offers *asymptotically favorable propagation* [32]

The favorable propagation situation in equation (1.4) does not only offer optimum efficiency with linear processing, but also reflects the most desirable situation for maximizing the data rate [33].

In a nutshell, favorable propagation cannot only improve the performance, but also simplify the massive MIMO system's algorithm design. The interuser or intercell interference can also be alleviated by the orthogonality, which helps to improve the capacity of the system [34]. The scheduling gain fast fading is also mitigated, which simplifies the scheduling scheme [34].

Convergence is the rate at which a massive MIMO system will achieve favorable propagation. Convergence enables us to know whether the massive MIMO channel achieves favorable propagation as a function of the system [35].

The convergence of massive MIMO systems to favorable propagation is measured using two key metrics defined as the Mean Absolute Deviation (MAD) and the Diagonal dominance (DD) [33–35]. From equation (1.4) and (1.5),

$$\frac{1}{M}\mathbf{G}^T\mathbf{G}^* = \frac{\mathbf{D}^{1/2}\mathbf{H}^T\mathbf{H}^*\mathbf{D}^{1/2}}{M} \to \mathbf{D}_\beta \tag{1.6}$$

As illustrated in equation (1.6), the channel can be said to have favorable propagation as the channel matrix approaches a diagonal matrix. The diagonal domi-

nance is therefore defined in [35] as the rate at which the sum of diagonal elements grow faster than the off-diagonals.

Also, from equation (1.6), it can be deduced that

$$\frac{1}{M}\mathbf{H}^T\mathbf{H} \rightarrow \mathbf{I} \tag{1.7}$$

Equation (1.7) also illustrates that as M increases, $\mathbf{H}^T\mathbf{H}^*/M$ approaches the identity matrix, $\mathbf{I}$. The Mean Absolute Deviation as defined in [35] is used to find the deviation of the channel matrix away from $\mathbf{I}$.

1.1.4 Massive MIMO Channel Models

The performance of massive MIMO systems is usually evaluated using two main channel models. They are the Correlation-Based Stochastic Channel Model (CB-SCM) and the Geometry-Based Stochastic Channel Model (GBSCM) [21].

CBSCMs are used for analyzing the theoretical performance of MIMO wireless communication systems. Examples of CBSCMs includes the Rayleigh Fading channel model, Rician Channel model and the Kronecker channel model [27].

Oftentimes, CBSCMs are not used for practical massive MIMO performance evaluation because they do not model large scale propagation characteristics as well as antenna parameters, which are needed for practical MIMO systems evaluation [27]. As a result, CBSCMs do not give an accurate reflection of massive MIMO system performances. Equation (1.8) shows an example of a CBSCM, (i.e. Kronecker channel model)

$$\mathbf{H} = \mathbf{R}_t^{1/2}\mathbf{H}_{iid}\mathbf{R}_r^{1/2} \tag{1.8}$$

where $\mathbf{H}$ represents the channel matrix, R_t and R_r denote the transmit and receive spatial correlation, respectively. $\mathbf{H}_{iid}$ represents the i.i.d. or uncorrelated channel matrix.

GBSCMs, on the other hand, accurately reflect the realistic channel properties of

wireless communication systems and are better suited for massive MIMO channel modeling performance [27]. GBSCMs include channel parameters that are useful for evaluating practical massive MIMO systems. GBSCMs can be further classified as 2D and 3D channel models.

The 2D channel model employs linear antenna arrays at the BS and it is capable of adapting in the azimuth domain only while the 3D channel model employs antenna arrays such as rectangular, cylindrical and spherical antenna arrays at the BS. 3D channel models are capable of adaptation in both azimuth and elevation domains [21]. The large scale propagation of 3D massive MIMO channel models include the Shadow Fading (SF), the Delay Spread (DS), the Azimuth of Arrival and Departure angles (AoA and AoD, respectively), as well as the Elevation of Arrival and Departure (EoA and EoD, respectively) [27]. An example of the 3D channel model based on WINNER+ and 3GPP is shown in equation (1.9) from [36, 37],

$$[\mathbf{H}_{s,u}] = \sum_{n=1}^{N} \alpha_n \sqrt{g_t(\phi_n, \theta_n, \theta_{tilt})} \sqrt{g_r(\varphi_n, \vartheta_n)} x [a_r(\varphi_n, \vartheta_n)]_u x [a_t(\phi_n, \theta_n)]_s \quad (1.9)$$

where $s = 1, ..., N_{BS}, u = 1, ..., N_{MS}, \alpha_n$ denotes the complex amplitude of the path, assumed to be a random variable. (ϕ_n, θ_n) are defined as the azimuth and elevation angles of departure (AoD), respectively. (φ_n, ϑ_n) represents the azimuth and elevation angles of arrival(AoAs) of the n^{th} path respectively.

1.2 Statement of Problem

So far, research done on the analysis of the convergence of massive MIMO systems to favorable propagation have examined the convergence properties using the CBSCM, which does not reflect the realistic practical performance of massive MIMO systems.

Moreover, the impact of the different antenna array topologies proposed for the massive MIMO technology on the convergence of massive MIMO to favorable

propagation have received little amount of research, and has also not been examined in practical channels. There has not also been adequate research done on the impact of varying the separation between the antenna elements, the angular spreads of the distribution of angles of arrival, as well as the azimuth and elevation spreads on the convergence, for different antenna array topologies. Even though research has shown that increasing the standard deviation of the distribution of angles of arrivals reduces the correlation among the antenna elements, its impact on the convergence performance has received little attention.

1.3 Aims and Objectives

1.3.1 General Objective

To investigate the rate of convergence of user channels to favorable massive MIMO propagation employing different antenna array topologies using a 3D GBSCM in different angular distributions based on the MPA concept.

1.3.2 Specific Objectives

1. Modify the WINNER+ and 3GPP channel which follows a GBSM and present a new channel realization when the transmitter is URA and CA.

2. Use SC expressions of URA and CA regarding Laplacian, Gaussian, Von Misses and Student's -t distributions based on the Maximum Power of Arrival to study its impact on the convergence of massive MIMO to favorable propagation.

3. Analyze the convergence using the Mean Absolute Deviation (MAD) and the Diagonal Dominance (DD).

4. Compare results to previously established results.

1.4 Methodology

1. Use MATLAB to compute and derive the spatial correlation coefficients for four different angular distributions (i.e Gaussian, Laplacian, Student's -t and Von Misses), and for each of the antenna array topology.

2. Use MATLAB to compute and generate the channel parameters for modeling the 3D Geomtery-based stochastic Channel Model.

3. Use MATLAB to evaluate the convergence metrics i.e. the Mean Absolute Deviation (MAD) and Diagonal Dominance (DD) for the 3G Geometry-Based channel model.

4. Employ the MAD and the DD to analyze and compare the performance in both correlated-based and geometry-based stochastic channel models.

1.5 Contents and Innovations of the Thesis

This work presents a standardized guideline of evaluating the convergence for URA and CA antenna topologies to massive MIMO favorable propagation under different angular distributions and thereby eliminates the need for separate generation of expressions for specific angular distributions. The work also presents the convergence performance in a practical 3D massive MIMO system, which gives a more accurate reflection of the performance.

1.6 Outline of the Thesis

The thesis is composed of six main chapters and it is organized as follows: Following the Introduction,

- Chapter 2 presents both the Literature review as well a theoretical review for this study. The literature review is in two segments. The first part

presents a review of literature on spatial correlation models and the second part of the literature review presents related works on convergence of massive MIMO systems. In the theoretical review, Key aspects of the study including the MPA concept are reviewed more in details.

- Chapter 3 presents the 3D massive MIMO channel model based on the MPA for the URA and CA antenna array topologies. The chapter then outlines the generation of the 3D massive MIMO channel parameters. In this chapter, the MPA concept is used to derive the SC characterization for different angular distributions of massive MIMO.

- Chapter 4 discusses the Massive MIMO system performance in both correlated-based and geometry-based stochastic channel model, for the two antenna array topologies. This chapter is then concluded with a performance comparison between the two different channels models as well as a comparison between the two different antenna arrays.

- Chapter 5 concludes the thesis with key contributions and possible future research directions.

Chapter 2

Literature Review and Concept of Maximum Power of Arrival

2.1 Massive MIMO

Massive MIMO system technology is primarily known for the exploitation of the spatial domain such that sufficiently diverse channel vectors can be obtained between each TX antenna and RX antenna pair [21, 22]. The number of independent channels between the antenna pairs is known as the multiplexing gain [21]. This multiplexing gain is equal to minimum number of the TX and RX antennas. Since the capacity of the system scales proportionally to the multiplexing gain [17], MIMO technology has been well studied over the past two decades and has now been labeled as one of the key technologies in current wireless system deployments [19].

2.1.1 System Model

For the general system model of the massive MIMO, a Multi-user MIMO (MU-MIMO) is considered, where a total of M transmitting antennas (TX) serves simultaneously K number of users. Let J represent the number of antennas on the downlink in a single time/frequency resource [38].

The J x 1 received vector, $\mathbf{y}$, for an arbitrary user can therefore be defined by equation (2.1),

$$\mathbf{y} = \sqrt{\rho}\mathbf{H}\mathbf{x} + \mathbf{v} \tag{2.1}$$

where $\mathbf{H}$ is the channel matrix of the J x M channel, $\mathbf{x}$ is the M x 1 precoded vector of data symbols $\mathbf{s}$, which is dependent on the type of precoder used at the

transmitter. $\mathbf{v}$ is the J x 1 i.i.d. additive white Gaussian noise (AWGN) vector with $\mathcal{CN}(0,1)$ entries. ρ denotes the received SNR at the user [35].

2.2 Channel Models

As mentioned in section 1.1.4 of this thesis, the two distinct channel models are primarily used for evaluating the efficiency of massive MIMO systems, which are the Correlation-based Stochastic Channel Model (CBSCM) and the Geometry-based Stochastic Channel Model (GBSCM). While the GBSCMs reflect the realistic characteristics of the channel, the CBSCMs are limited for practical massive MIMO system. Table 2.1 presents a summary of the current channel models used.

Table 2.1: Channel Models of Massive MIMO

Method of Modeling	Category	Property
CBSCM	i.i.d. Rayleigh Fading channel model	The fast fading elements are i.i.d. complex Gaussian variables.
	The correlation channel model	Contains correlation between transmit and / or receive antennas.
GBSCM	2D channel model	Propagates beams in the 2D plane, such as the linear array.
	3D channel model	Propagates beams in the 3D plane, such as rectangular, cylindrical and spherical array.

2.2.1 Correlation-Based Channel Models

Generally, the analysis assumes that user equipment (UEs) uses single antennas, taking into account the complexity and space of low carrier terminal equipment [3]. In the analysis of CBSCMs, UEs using single antennas are employed and this can easily be extended to the case where the UE uses multiple antennas. CBSCMs are further streamlined into three distinct channel models according to the fast fading matrix, namely the i.i.d. Rayleigh fading channel model, the correlation channel model and the [27] mutual coupling channel model. The three models of channels are discussed in detail as follows.

i.i.d. Rayleigh Fading channel model

This channel model is commonly used in massive MIMO systems for theoretical assessment. In this model, it is assumed that there is no correlation between transmitting antennas or receiver antennas and mutual connection [37]. The elements of the fast-fading matrix denoted as $\mathbf{H} = [\mathbf{h}_1, \mathbf{h}_2, ..., \mathbf{h}_K]$ are i.i.d. Gaussian random variables, thereby $h_{n,k} \sim \mathcal{CN}(0,1)(n = 1, 2, ..., N; k = 1, 2, ..., K)$.
Rayleigh fading channel can also be used to model rich scattering environments such as those at microwave bands and the non-line-of-sight (NLOS)/diffuse component of a Rician fading channel [29]. It is the simplest channel model and allows closed form analysis in many applications [27].

Correlation channel model

The correlation channel model represents the antenna correlation induced by inadequate antenna spacing and scattering surroundings and is thus used to assess the efficiency of huge MIMO systems [37]. Each UE's fast fading vector can be obtained by multiplying the correlation matrix by a standard complex Gaussian vector [27]. This is illustrated in equation (2.2)

$$\mathbf{h}_k = \mathbf{R}_k \mathbf{v}_k, \quad k = 1, 2, ..., K \tag{2.2}$$

where the steering matrix, defined as $\mathbf{R}_k \in \mathcal{C}^{NxD_k}$ contains D_k steering vectors with different angles of arrival (AoAs) for the kth UE and $\mathbf{v}_k \sim \mathcal{CN}(0, 1_D)$
When linear array is employed at the eNB, the steering matrix $\mathbf{R}_k$ can be written as

$$\mathbf{R}_k = \frac{1}{D_k}[\mathbf{a}(\theta_{k,2}), \mathbf{a}(\theta_{k,2}), ..., \mathbf{a}(\theta_{k,D})], \tag{2.3}$$

where $\theta_{k,i}$ is the ith AoA of the kth UE. The steering vector, $\mathbf{a}(\theta_{k,1}) \in \mathcal{C}^{Nx1}$ is given as

$$\mathbf{a}(\theta_{k,1}) = [1, e^{(j2\pi d/\lambda) sin\theta_{k,i}}, ..., e^{(j2\pi(N-1)d/\lambda) sin\theta_{k,i}}]^T, \tag{2.4}$$

Where d defines the wavelength of the carrier between the adjacent antennas and λ. The steering vector can be achieved in the event of the rectangular antenna array, as demonstrated in equation (2.5) as

$$\mathbf{a}(\theta_{k,i}, \theta_{k,i}) = vec\{[1, e^{(j2\pi d/\lambda)sin\theta_{k,i}}, ..., e^{(j2\pi(N-1)d/\lambda)sin\theta_{k,i}}]^T\}\otimes$$

$$vec\{[1, e^{(j2\pi d/\lambda)sin\theta_{k,i}}, ..., e^{(j2\pi(N-1)d/\lambda)sin\theta_{k,i}}]\} \tag{2.5}$$

where $\theta_{k,i}$ and $\theta_{k,i}$ represents the azimuth of arrival (AoA) and elevation of arrival (EoA) respectively and $vec\{.\}$ denotes the vectorization matrix.

This correlation channel model introduces the AoAs that can be used to differentiate different UE and improve channel estimation accuracy [39]. The UE channels can be almost segregated by angle data when the UE is situated at distinct orientations, thereby alleviating the contamination of the pilot. It is also useful in the analysis of intercell or inter-user interference and in the development of UEs scheduling or cell cooperation to alleviate interference [39].

Mutual coupling channel model

Since the number of antennas in the massive MIMO system increases to a large scale, due to the limited space of the antenna array, the mutual impedance must also be taken into account. [40]. In addition, to reflect the realistic channel model, the load impedance and antenna impedances should also be characterized. The kth UE channel vector can be written as shown in equation(2.6) taking both impedances and correlation into account [41],

$$\mathbf{h}_k = \mathbf{Z}\mathbf{R}_k\mathbf{v}_k, \quad k = 1, 2, ..., K, \tag{2.6}$$

where $\mathbf{Z} \in \mathcal{C}^{NxN}$ represents the mutual coupling matrix and $\mathbf{R}_k \in \mathcal{C}^{NxD}$ denotes the steering matrix containing $\mathbf{D}_k$ steering vectors of the receiver antenna array, and $\mathbf{v}_k \sim \mathcal{CN}(0, 1)$. According to [40, 41], the mutual coupling matrix can be

expressed as

$$\mathbf{Z} = (Z_A + Z_L)(\Gamma + Z_L\mathbf{I})^{-1} \tag{2.7}$$

with

$$\Gamma = \begin{bmatrix} Z_A & Z_M & 0 & ... & 0 \\ Z_M & Z_A & Z_M & ... & 0 \\ 0 & Z_M & Z_A & ... & 0 \\ . & . & . & . & . \\ . & . & . & . & . \\ . & . & . & . & . \\ 0 & 0 & ... & Z_M & Z_A \end{bmatrix} \tag{2.8}$$

where Z_M, Z_A and Z_L represent the mutual impedances, antenna impedances and the load impedances respectively. In this case, only between the adjacent antennas, which can be seen from the nonzero Z_M, are the mutual impedances considered. The matrix of transmission correlation can therefore be written as shown in equation (2.9) as The transmission correlation matrix is therefore represented as shown in equation (2.9) [29],

$$\Sigma_N = E[\mathbf{H}\mathbf{H}^H] = K\mathbf{Z}\mathbf{R}\mathbf{R}^H\mathbf{Z}^H \tag{2.9}$$

where $\mathbf{R} = [\mathbf{R}_1, \mathbf{R}_2, ..., \mathbf{R}_K]$. As the UE is geometrically distributed, it is assumed that the received correlation matrix to be $\mathbf{I}_K$ which evaluates $\mathbf{H}$ as $\mathbf{H} \sim \mathcal{CN}(0, \Sigma_N \otimes \mathbf{I}_K)$.

One advantage that the mutual coupling channel model brings about is that, as compared to the correlation and Rayleigh channel models, it is practical and more suitable for massive MIMO. It is also useful in evaluating the impacts of antenna spacing on the efficiency of huge MIMO devices, which is important in the setup of antenna arrays, particularly sparse antenna arrays [27].

2.2.2 Geometry-Based Channel Model

GBSCMs can be categorized into two different types: 2D and 3D channel models [21].

The tilt angle is generally held constant with the use of the Uniform Linear Array (ULA) used at the eNB and the 2D channel model is exactly enough to evaluate the efficiency of the massive MIMO scheme. However, if the eNB uses 3D antenna arrays such as the spherical array, rectangular array or the cylindrical array configurations, the 3D channel model that considers both the elevation and the azimuth should be used for evaluation [37]. The 3GPP channel model is standardized for frequencies below 6 GHz and can be used to model urban micro, urban macro as well as suburban macro cells, both for 3D indoor/outdoor scenarios [43]. Due to the complexity in generating the channel model parameters and the fact that it is based on extensive measurement campaigns, carried out by the 3GPP, the channel model is typically only used for detailed simulation purposes [42, 43].

However, if the eNB uses 3D antenna arrays such as the spherical array, rectangular array or cylindrical antenna array configurations, the 3D channel model that considers both the elevation and the azimuth should be used for evaluation. [44–46]. The properties are useful in decorating the channels for different UE types, thus providing a favorable channel [47, 48]. However, they increase the trouble for the massive MIMO scheme to set up the channel model. Like [49–51], it is also possible to observe the non-stationary phenomenon by measuring the linear 128-antenna array in a semi-urban region. [52].

The generation of channel parameters for the 3D massive MIMO channel model is outlined in detail in [53–55] based on WINNER+ 3GPP. The 3D channel model's primary parameters include shadow fading (SF), delay spread (DS), the K factor, both AoA, azimuth starting angles (AoD), EoA, and starting elevation angles (EoD), particularly the EoA and EoD [51, 55]. The 3GPP Release 12 (R12), defined three different environment scenarios which include the urban microcell with

high UE density (3D-UMi), urban macrocell with high UE density (3D-UMa), and the urban macrocell with one high-rise per sector and 300m intersite The 3D MIMO channel's large-scale propagation comprises of both Pathloss and shadow fading. Taking into account the various propagation environments [54], the path loss model can be classified as outdoor or outdoor-to-indoor (O2I) models.

2.3 Maximum Power of Arrival of Distributions

The Maximum Power of Arrival can be defined as follows: If the real distribution of power as a function of $u = sin\xi$ is given by $p(u)$ and the phase gradient of the incident wave is proportional to u, where ξ represents phase angle of the incident wave, then the maximum power is relative to distribution of true power and this is given in equation (2.17) as

$$P_{max} = \int_u p(u)du \tag{2.10}$$

Having defined the MPA of distribution of AoA in equation (2.18) the concept is extended to determine the MPA distributions for the Student's t-distribution, Laplacian, Gaussian, Von Mises and arbitrary Q- power cosine distributions.

2.3.1 Maximum Power of Laplacian Distribution

The field measurement data shows, as illustrated in [67], that the angle-of-arrival (AOA) distribution in general has a shape resembling a Laplacian and Gaussian distribution. The Laplacian distribution is given as

$$P_{lap}(\zeta) = C_l e^{-a|\alpha_l - \zeta|} - \pi + \alpha_l \leq \zeta\pi + \alpha_l \tag{2.11}$$

where $C_l = a/2(1 - e^{a\pi})$ is the normalizing constant, ξ is the phase angle and a represents the decay factor which varies inversely to the angle of the spread and α_1 defines the central AoA. The maximum power of arrival can thus be express

as

$$P_{max}^{lap} = \int C_l e^{-a|\sigma_l - \xi|} d\xi = (1/a) C_l e^{-a|\alpha_1 - \zeta|} \tag{2.12}$$

2.3.2 Maximum Power of Gaussian Distribution

As illustrated for the Laplacian distribution, the Gaussian distribution is expressed as

$$P_{gauss}(\zeta) = \frac{\kappa}{\sigma\sqrt{2\pi}} e^{-(\zeta-\alpha_a)^2/2\sigma^2}, \quad -\pi + \alpha_a \leq \zeta\pi + \alpha_a \tag{2.13}$$

where σ and α_a are defined as the standard deviation and mean direction of arrival of the distribution respectively. And

$$\kappa = \frac{1}{(efrc(\pi/\sigma\sqrt{2})} \tag{2.14}$$

is the normalization factor which makes $P_gauss(\zeta)$ a physical density function. And

$$erf(x) = \frac{2}{x} \int_0^x e^{t^2} dt \tag{2.15}$$

is the error function. It is worth noting that κ is equivalent to unity when the angular spread is small. The maximum power is given by

$$P_{max}^{gauss}(\zeta) = \frac{\kappa}{\sigma\sqrt{2\pi}} \int e^{-(\zeta-\alpha_a)^2/2\sigma^2} d\zeta = \frac{\kappa\sigma}{\sigma\sqrt{2\pi(\zeta - \alpha_a)}} \int e^{-(\zeta-\alpha_a)^2/2\sigma^2} d\zeta \tag{2.16}$$

2.3.3 Maximum Power of Von Misses Distribution

The Von Misses model was first presented in 1918 to model the contrasts between the theoretical measured atomic weights by German physicists Richard Von Misses [68]. For a unit vector of dimension, the Von Misses probability density function is given as

$$P_p(x; \mu\kappa) = C_p(\kappa) e^{\kappa\mu^T x} \tag{2.17}$$

where T signifies the matrix transposition operator, mean direction is represented by μ. The κ defines the accumulation of the distribution and C_p is a normalizing constant given as

$$C_p(\kappa) = \frac{\kappa^{p/(2-1)}}{(2\pi)^{p/2} I_{p(2-1)}(\kappa)} \tag{2.18}$$

in which I_v denotes the modified Bessel function of the first order and kind, v. In an urban environment where the angle of arrival ζ component results from the multipath propagation, the Von Misses distribution is expressed as

$$P_{von}^{max}(\zeta) = \frac{1}{2\pi I_o(\kappa)} e^{\kappa cos(\zeta - \zeta_m)}, \quad -\pi + \zeta_m \leq \pi + \zeta_m \tag{2.19}$$

where ζ_m is the mean direction of a set of directional components which ranges in the interval $[0, \pi]$

2.3.4 Maximum Power of Student's t-distribution

The Student's t-distribution can be defined as the distribution of $u = sin\zeta$. The probability density function (pdf) of this distribution in the $u-$ space is expressed as [63]

$$P_{std}(u) = \frac{1}{2} \frac{\mu^2}{\mu^2 + (u^2 + (u - \sqcap)^2)^{3/2}} \tag{2.20}$$

where μ denotes the measure of angular spread and ζ is the angle of arrival. Applying the MPA concept,

$$P_{max}^{std}(\zeta) = \frac{1}{2\mu} \int \frac{cos\zeta}{(1 + m^2 sin^2\zeta)^{3/2}} d\zeta \tag{2.21}$$

2.4 Review of related works on Spatial Correlation models

In [59], researchers have shown that 3D MIMO enables the efficient utilization of the spatial resources. Without adequate modeling and planning of channel

characteristics using elevation, however, all these benefits can not be achieved. Unlike the two-dimensional (2D) spatial correlation of antenna arrays, the 3D SC of antenna arrays allows elevation spread into the 3D channel model and antenna configuration to access and use all the degrees of flexibility the channel offers [60]. This is because the real world nature of transmission in 3D MIMO requires both azimuth and elevation spreads to enhance spectrum efficiency and improve network throughput completely. It is an existing fact that the 3D SC between antenna positions on array geometry is a function joint distribution of the azimuth and the elevations spreads of the incident wave [61, 62]. Given this, it is not an overstatement for one to conclude that the variations in the parameters of angular distribution will influence the 3D SC between antenna positions. However, the classic work done by Andersen and Pedersen in [63] has led to the emergence of several characterizations of 3D SC using uniform angle-of-arrival (AOA) probability density function (pdf). Researchers in [64] considered the uniform AOA to derive the spatial fading correlation models for ULA, UCA and URA compact MIMO receivers. Authors indicated that the proposed SC models were useful in determining the covariance matrix at both the transmitter and receiver for performance evaluation. Moreover, authors examined the impacts of the angular parameters associated with azimuth spread (AS), mean elevation of arrival (MEOA), elevation spread (ES) and the mean azimuth of arrival (MAOA) on MIMO performance. The analytical expression assumed uniform AOA and is expressed as a function of azimuth and elevation angles of arrival as well as the polarization states of the wave. The results obtained could be used to determine the SC matrix on both sides of the transmitter and receiver in multiple-input-multiple-output systems. In [65], approximate SC expressions of ULA and UCA using cluster channel models MIMO have been derived. Further, authors demonstrated the possibility of avoiding numerical integrals and compare parametric and non-parametric channel models. They also demonstrated that the suggested model fits perfectly with current low-angle spread parametric models. As already

stated, field measurement information indicates that the AOA distribution generally has a shape that looks like a Laplacian and Gaussian distribution [66, 67]. Therefore, authors in [62, 65] have derived the 3D SC of antenna arrays using Laplacian and Gaussian distributions useful for MIMO performance evaluation. In [67], authors derived a SC expression of UCA using the Laplacian distribution. Using computer simulations authors obtained a perfect match between theoretical and simulation results. The correlation between antenna elements reduced as the separation increased. Moreover, using Gaussian angle and spatial distributions the SC functions of ULA and UCA were derived in [62] for assessment of MIMO performance. Other researchers have also proposed the Von Mises and arbitrary Q- power cosine distributions [68, 69] that was first introduced to model the non-isotropic propagation mechanism. Using a different method such as the spherical harmonic expansion (SHE) of planewaves, an expression for the SC for the uniform AOA pdf was presented in [70]. Researchers in [71] have also shown on accounts of large-scale transmitters such as the cylindrical array (CA) that the spatial correlation matrix can be expressed in zenith and azimuth directions as the Kronecker product of each correlation matrix. Following this development, approximate antenna architecture expressions for SC were developed using Fourier transforms to investigate correlated channel convergence properties.

2.5 Review of related works on Convergence

Authors in [35] looked at the convergence characteristics of huge MIMO schemes by examining the amount of antennas needed for huge MIMO benefits. This work analyzed the convergence properties using a Rayleigh fading channel model.

In this work, three convergence metrics were defined as follows; Mean Absolute Deviation (MAD), Eigenvalue Ratio (λ ratio) and Diagonal Dominance (DD). These metrics were evaluated based on a number of scenarios; In the first scenario, K is fixed as $M \to \infty$ and in the second scenario, $\frac{K}{M} = \alpha^{-1}, K \to \infty, \alpha$ is fixed. This work demonstrated that the λ ratio converges to 1 when M is excess of 10^4 as

K is fixed at 10 and 50. The work further illustrated that difference of the Mean Absolute Deviation (MAD) of $\mathbf{H}^T\mathbf{H}^* vs M$ away from the identity matrix, $\mathbf{I}$ quickly approaches zero for M number of antennas in excess of 500. This work further concluded that, the channel matrix becomes increasingly diagonal dominant for fixed number of users, K but became less diagonal dominant as both K and M were allowed to increase. Approximate expressions of the spatial correlations of Cylindrical Array (CA) and Uniform Rectangular Arrays (URA) were also derived from researchers in [72] using measured angle departure distributions (AoD) for both zenith and azimuth. This work further examined the convergence of the antenna arrays using the Rayleigh fading channel model and the Kronecker correlation model. Different results are obtained between the correlated scenarios of antenna arrays and i.i.d. situations. Corresponding to the outcome in [72], the i.i.d scenario declines to zero faster than the correlated scenarios with a quicker convergence rate at larger α for an increase of K. This happens only in the uncorrelated channel when the value of W approaches I_K. In the correlation scenario, the effect of correlation alter the values of W thus the values are not close to I_K. It is then not unexpected that the outcome of the correlation scenario will converge. In addition, [72] concluded that while the massive MIMO show convergence for a large antenna numbers for the i.i.d. channels, the desirable massive MIMO properties are degraded by the presence of spatial correlation.

2.6 Motivation

The focus in all the above has been on studying the convergence of massive MIMO in CBSCM. Little has been done on the effect of antenna parameters and SC on convergence in both CBSCM and GBSCM regarding different angular distributions. There is therefore the need to investigate the effect of increasing the azimuth (AS) and elevation (ES) spreads of the angular distributions of arrival and antenna element spacing on the rate of convergence of massive MIMO for both CBSCM and GBSCM.

Chapter 3

Methodology

Chapter three discusses the system model and the channel models of the proposed massive MIMO system. It also introduces the MPA concept as it is implemented for massive MIMO performance to achieve the 3D SC expressions of both the Uniform Rectangular Array (URA) and the Cylindrical Array (CA). The chapter also presents the MPA of AOA distributions for the Student's t-distribution, Laplacian, Gaussian, and Von Mises distributions.

3.1 System Model

In this thesis, a massive MIMO system employing several numbers of antennas, M serving simultaneously single-antenna users, K is considered. Time division duplex (TDD) mode is regarded with uplink pilots allowing downlink channel estimation by the transmitter. The K terminals receive a K x 1 vector as defined in equation (3.1) on the downlink (where TDD is assumed).

$$\mathbf{x}_f = \sqrt{\rho f}\mathbf{G}^T\mathbf{s}_f + \mathbf{w}_f \tag{3.1}$$

where ρ_f denotes the transmit SNR, $[.]^T$ represents matrix transpose and s_f defines an M x 1 precoded vector of data symbols. w_f represent a K x 1 noise vector with an i.i.d. $\mathcal{CN}(0,1)$. The M x K channel matrix, $\mathbf{G}$, is represented by

$$\mathbf{G} = \mathbf{H}\mathbf{D}_{\beta}^{\frac{1}{2}} \tag{3.2}$$

where $\mathbf{H}$ is a M x K channel matrix that accounts for the small-scale Rayleigh fading and the spatial correlation effect and $\mathbf{D}_\beta$ defines the diagonal matrix mod-

eling large-scale effects. The $\mathbf{D}_\beta$ diagonal components are depicted by a K x 1vector, β, representing the β_j link gains. This is represented by

$$\mathbf{D} = diag[\beta_1, \beta_2, ..., \beta_K] \tag{3.3}$$

The correlation also improves as the number of antennas rises in massive MIMO. In this thesis, the analysis considered only the transmitter's spatial correlation. Therefore, the correlated channel, defined as $\mathbf{H}$ models the transmit spatial correlation, R_t and $\mathbf{H}_{iid}$ which represents the independent and identically distributed (i.i.d.) channel matrix. This is illustrated in equation (3.4)

$$\mathbf{H} = \mathbf{H}_{iid} R_t^{1/2} \tag{3.4}$$

3.2 Channel Model and Antenna Configuration

In this section, the antenna configuration of 3GPP standards and WINNER+ model used for the MIMO channel modeling for this study is presented. The section also presents a link between the base station (BS) and the mobile station (MS). For this thesis, the WINNER+ and 3GPP standards were considered because research has recognized that a substantial energy component is radiated in the elevation domain. [52]. The description of the propagation route in the azimuth domain does not therefore only improve the efficiency [27]. Elevation and azimuth angles at the BS are denoted by θ_n and ϕ_n respectively. That of the MS is represented by ϑ_n and φ_n respectively. The BS is modeled as URA or UCA.

The effective channel between the BS antenna port and the MS antenna port is provided in accordance with 3GPP standards as

$$[\mathbf{H}_{s,u}] = \sum_{n=1}^{N} \alpha_n \sqrt{g_t(\phi_n, \theta_n, \theta_{tilt})} \sqrt{g_r(\varphi_n, \vartheta_n)} \times [a_r(\varphi_n, \vartheta_n)]_u \times [a_t(\phi_n, \theta_n)]_s \tag{3.5}$$

where $s = 1, ..., N_{BS}, u = 1, ..., N_{MS}, \alpha_n$ is defined as the complex amplitude of the path, assumed to be a random variable. (ϕ_n, θ_n) represent the azimuth and elevation angles of departure (AoD), respectively. (φ_n, ϑ_n) are the azimuth and elevation angles of arrival(AoAs) of the n^{th} path respectively. One advantage of the 3D channel model in equation (3.7) is the introduction of θ_{tilt} the down-tilt angle of the antenna. This is because keeping the elevation angle of the antenna boresight to be fixed does not exploit the channel's degrees of freedom in the elevation. [36]. The dynamic adjustment of the downtilt angles can open up numerous potentials for the 3D beamforming which can lead to substantial performance improvements [43]. The vectors $a_t(\phi, \theta)$ and $a_r(\varphi, \vartheta)$ are the array response of the BS and MS, respectively. Their entries are expressed as,

$$[a_t(\phi, \theta)]_s = exp(i\psi_t.x_s) \tag{3.6}$$

$$[a_r(\varphi, \vartheta)]_u = exp(i\psi_r.x_u) \tag{3.7}$$

where x_s and x_u denotes the location vectors of the s^{th} and u^{th} transmit (TX) and receive (RX) antennas, respectively. ψ_t and ψ_r represent the transmit and receive wave vectors, where $\psi = kv$, with $k = \frac{2\pi}{\lambda}$, and λ is the wavelength which signifies the direction of wave propagation. According to [38]

$$g_t(\phi_n, \theta_n, \theta_t ilt) \approx g_t, H(\phi_n) g_t, V(\theta_n, \theta_t ilt) \tag{3.8}$$

where $g_t, H(\phi_n)$ and $g_t, V(\theta_n, \theta_{tilt})$ are the vertical and horizontal antenna patterns at the transmitter and are approximated in dB as

$$g_t, H(\phi) = -12(\frac{\phi}{\phi_{3dB}})^2 dB \tag{3.9}$$

$$g_t, V(\theta, \theta_{tilt}) = -12(\frac{\theta - \theta_{tilt}}{\theta_{3dB}})^2 dB \tag{3.10}$$

where θ_{3dB} illustrates the vertical and horizontal 3dB beamwidths, respectively.Also, the individual MS radiation pattern, gr, φ, ϑ, is taken as 0 dB because the MS does not generally favor any direction.

3.2.1 Generation of 3D massive MIMO channel model for Cylindrical Array

The configuration for the CA can be obtained by wrapping a URA around a virtual cylinder as depicted in Figure 1.5. The CA is therefore modeled in the analysis as an A-element ULA (Figure 1.1) in the direction of z (zenith domain) and B-element in the direction of x, y (azimuth domain). The location vector of the sth transmit (Tx) can be obtained by knowing the position of mth UCA in the direction of z and the angular position of the nth element on the mth UCA in the x, y plane where $m = 1, ..., M$ represents the total number of UCA elements in the direction of z and $n = 1, ..., N$ denotes the total number of antenna elements on each UCA. Provided that the CA antenna array dimension is $l = 4\lambda$, the cylinder radius and UCA can be defined as $\rho = 4\lambda/l$. If $d_z = 4\lambda/M$ wavelengths represents the distance between the first and second UCA in the z direction, then the third and the subsequent position of the UCA will be $4\lambda(m-1)/M$ wavelengths. As illustrated in [26], the angular position of the nth element of the mth UCA on the x, y plane is $\varphi_s = 2\pi(n-1)/N$ and the location vector can be represented as $v_t.x_s = cos(\phi - \varphi_s)sin\theta$. In considering the assumptions above, the array response of the sth BS antenna port of CA using Eq. (26) is given by

$$[a_r(\varphi_n, \vartheta_n)]_u = exp(ik(u-1)drsin\varphi sin\vartheta) \tag{3.11}$$

LTE antenna ports are considered at the MS to support different transmission modes described in [42]. Each antenna port behaves like a single antenna with this configuration, since its elements carry the same identical signal. The array response of the uth MS antenna port in connection with the 3-D channel model

can be expressed as [62]

$$[a_r(\varphi_n, \vartheta_n)]_u = exp(ik(u-1)drsin\varphi sin\vartheta) \tag{3.12}$$

The resultant 3-D channel realization between the sth TX antenna port of CA and the single antenna RX port is derived as

$$[\mathbf{H}_{s,u}]_{CA} = \sum_{n=1}^{N} \alpha_n \sqrt{g_t(\phi_n, \theta_n, \theta_{tilt})} exp(ik\rho(4\lambda(m-1)/M)cos(\phi_n - \varphi_s)sin\theta_n) \times \sqrt{g_r(\varphi_n, \vartheta_n)} exp(ik(u-1)drsin\varphi sin\vartheta) \tag{3.13}$$

where k represents the wave number and dr is the separation between the RX antenna ports.

3.2.2 Generation of 3D massive MIMO channel model for Uniform Rectangular Array

In the URA analysis, the response of the s^{th} BS antenna port of the URA antenna can be expressed in the scalars z and y - axes as

$$[a_t(\phi_n, \theta_n)]_s = exp(ikzcos(\phi_n - \gamma_s)sin\theta_n) \tag{3.14}$$

where the location vector of s^{th} element of URA at the BS is expressed as

$$v_t.x_s = cos(\phi_n - \gamma_s)sin\theta \tag{3.15}$$

Moreover, the parameters z and γ_s are also defined in this thesis as follows,

$$z = \sqrt{(z_x^2 + z_y^2)} \tag{3.16}$$

$$z_x = {}^{2\pi d_x(n-m)}/_{\lambda} \tag{3.17}$$

$$z_y = {}^{2\pi d_y(n-m)}/_{\lambda} and \tag{3.18}$$

$$\gamma_s = tan^{-1}({}^{z_x}/_{z_y}) \tag{3.19}$$

Considering the array response of the LTE antenna ports representing the MS ports defined in equation(3.16), The resultant 3D MIMO channel realization between s^{th} transmit (TX) antenna port of URA and the u^{th} receive(RX) port is then given by

$$[\mathbf{H}_{s,u}]_{URA} = \sum_{n=1}^{N} \alpha_n \sqrt{g_t(\phi_n, \theta_n, \theta_{tilt})} exp(ikzcos(\phi_n - \gamma_s) sin\theta_n) \times \sqrt{g_r(\varphi_n, \vartheta_n)} exp(ik(u-1)drsin\varphi sin\vartheta) \tag{3.20}$$

3.3 Generation of parameters for the 3D channel Model

3.3.1 Generation of Channel Coefficients

In the generation of the channel coefficients, the 2D channel model developed by the 3GPP was extended to a 3D channel model to include the effect of the elevation plane and antenna boresight. The signal obtained at the MS comprises of the transmitted signal's N time-delayed multipath replicas. The N paths are defined by the power and delay and are selected randomly according to the procedure of channel generation. Each path consists of M sub-paths. The channel modeling method for generating channel parameters for the 3D channel model is based on the MIMO spatial channel model for the 3GPP Technical Specification Group Radio Access Network (3GPP TR 25.996 version 15.0.0) [42].

3.3.2 Application Environment

To efficiently analyze the performance of massive MIMO systems utilizing the GBSCM, this section presents details of the application environment of the WINNER+ and the 3GPP standard employed. This study considered Urban Macro (3D-UMa) as the application environment. However, it has similar features as Urban Micro (3D-UMi) [32]. The two situations are considered to be densely populated concerning the buildings. It may be accepted that there is a more random distribution of the building blocks while the height of the building are generally distributed between four and eight floors. This is approximately 1.5 meters to 22.5 meters according to the WINNER+ and 3GPP standards in [42]. In the case of 3D-UMa, the base station height of twenty-five (25m) is presumed to be well above the heights of the neighboring buildings so that the central propagation mechanism for indoor and outdoor user equipment (UE) diffracts over the rooftop. On 3D-UMi accounts, the BS height of 10m is assumed to fit below the height of surrounding buildings. Hence, the signal strength received at the UE incorporates commitments from the rooftop as well as the building propagation mechanisms. Figure 3.2 presents the WINNER + and 3GPP features for 3D Channel model.

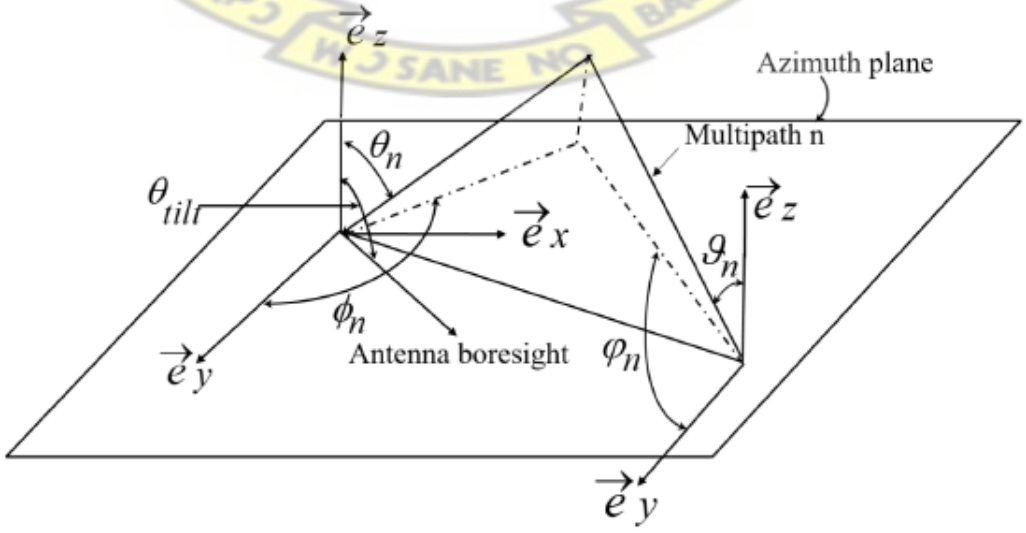

Figure 3.1: 3D Channel Model

3.4 Expressions of the Spatial Correlation based on MPA for Uniform Rectangular Array and Cylindrical Array

Having defined the MPA of distribution of AoA in section 2.4, the concept is extended to determine the MPA of offset distributions for the Student's t-distribution, Laplacian, Gaussian and Von Misses distributions.

3.4.1 Spatial Correlation Based on Maximum Power of Laplacian Distribution

$$\rho_{[(n,m),(m,q)]} = \frac{8\pi}{Zsin\theta} P_{max}^{lap}(\zeta) sin(Zsin\theta) \tag{3.21}$$

where P_{max}^{lap} is the maximum power of the Laplacian distribution evaluated in equation (2.19). Therefore the MPA for Laplacian distribution is defined as

$$\rho_{[(n,m),(m,q)]} = \frac{8\pi}{Zasin\theta} C_l e^{-a|\alpha_1 - \theta sin(\gamma+\phi)|} sin(Zsin\theta) \tag{3.22}$$

3.4.2 Spatial Correlation Based on Maximum Power of Gaussian Distribution

$$\rho_{[}(n,m),(m,q)] = \frac{8\pi}{Zsin\theta} P_{max}^{gau}(\zeta) sin(Zsin\theta) \tag{3.23}$$

where P_{max}^{gauss} is the maximum power of the Gaussian distribution evaluated in equation (2.23). Therefore the MPA for Laplacian distribution is defined as

$$\rho_{[(n,m),(m,q)]} = \frac{8\pi}{Zsin\theta} \times \frac{\kappa\sigma}{\sqrt{2\pi}(\theta sin(\gamma+\phi) - \alpha_a)} e^{-(\theta sin(\gamma+\phi)-\alpha_a)^2/2\sigma^2} sin(Zsin\theta) \tag{3.24}$$

3.4.3 Spatial Correlation Based on Maximum Power of Von Misses Distribution

$$\rho_{[}(n,m),(m,q)] = \frac{8\pi}{Zsin\theta} P_{max}^{von}(\zeta) sin(Zsin\theta) \tag{3.25}$$

where P_{max}^{von} is the maximum power of the Von Misses distribution evaluated in equation (2.26). Therefore the MPA for Laplacian distribution is defined as

$$\rho_{[(n,m),(m,q)]} = \frac{8}{Z2I_0(\kappa)sin\theta} sin(\theta sin(\gamma+\phi) - \zeta_m) e^{\kappa cos(\theta sin(\gamma+\phi)-\zeta_m)} sin(Zsin\theta) \tag{3.26}$$

3.4.4 Spatial Correlation Based on Maximum Power of Student's t-distribution

$$\rho_{[}(n,m),(m,q)] = \frac{8\pi}{Zsin\theta} P_{max}^{std}(\zeta) sin(Zsin\theta) \tag{3.27}$$

where P_{max}^{std} is the maximum power of the Von Misses distribution evaluated in equation (2.28) Therefore the MPA for Laplacian distribution is defined as

$$\rho_{[(n,m),(m,q)]} = \frac{4\pi}{Z\mu sin\theta} \left(\frac{sin(\theta sin(\gamma+\phi))}{2}(1 + m^2 sin^2(\theta sin(\gamma+\phi)))\right) sin(Zsin\theta) \tag{3.28}$$

3.5 Matlab Simulation

MATLAB (Matrix Laboratory), a numeric computing programming language, was implemented and used for the generation of the channel parameters as well as the computation of the convergence metrics.

In the simulation, the Urban Micro Environment parameters were considered as shown in Table (3.2).

Table 3.1: Angular parameters used for modeling [42]

Parameter	Description
Φ_{BS}	Array orientation of BS antenna
θ_{BS}	Direction of azimuth AoD LoS between the MS and BS
ϕ_{BS}	Direction of elevation AoD LoS between the MS and BS
$\delta_{n,AoD}$	nth path AoD for $(n = 1, ..., N)$ with respect to the LoS AoD θ_0.
$\triangle_{n,m,AoD}$	Offset of mth subpath $(m = 1, ..., M)$ for the nth path with respect to $\delta_{n,AoD}$.
$\theta_{n,m,AoA}$	Absolute azimuth AoD of the nth $(m = 1, ..., M)$ subpath for the nth path at the BS with respect to BS broadside.
$\phi_{n,m,AoA}$	Absolute elevation AoD of the nth $(m = 1, ..., M)$ subpath for the nth path at the BS with respect to BS broadside.
Φ_{MS}	Orientation of MS antenna.
θ_{MS}	The azimuth angle between the BS-MS LoS and the broadside of the MS.
ϕ_{MS}	The elevation angle between the BS-MS LoS and the broadside of the MS.
$\delta_{n,AoA}$	AoA for nth $(n = 1, ..., N)$ path, with respect to the LOS AoA $\theta_{0,MS}$.
$\triangle_{n,m,AoA}$	Offset of the mth $(m = 1, ..., M)$ subpath for the nth path with respect to $\delta_{n,AoA}$.
$\theta_{n,m,AoA}$	Absolute azimuth AoA denoting the mth $(m = 1, ..., M)$ subpath for the nth path at the MS with respect to the broadside of the BS
$\phi_{n,m,AoA}$	Absolute elevation AoA denoting the mth $(m = 1, ..., M)$ subpath for the nth path at the MS with respect to the broadside of the BS
v	vector of MS velocity.
θ_v	Velocity vector angle with respect to the broadside of MS: $\theta_v = arg(v)$

Table 3.2: 3GPP Environment Parameters [42]

Channel Scenario	Urban Macro Environment
Number of Paths(N)	6
Number of sub-paths (M) per path	20
Mean AS at BS AS at BS as a log-normal RV $\sigma_{AS} = 10^(\epsilon_{AS}x + \mu_{AS}), x \sim \eta(0,1)$	E($\sigma_{AS} = 15°$) $\mu_{AS} = 1.18$ $\epsilon_{AS} = 0.210$
$r_{AS} = \frac{\sigma_{AoD}}{\sigma AS}$	1.3
Mean ES at BS ES at BS as a log-normal RV $\sigma_{ES} = 10^(\epsilon_{ES}x + \mu_{ES}), x \sim \eta(0,1)$	E($\sigma_{ES} = 8°$) $\mu_{ES} = 0.810$ $\epsilon_{ES} = 0.34$
$r_{ES} = \frac{\sigma_{AoD}}{\sigma ES}$	1.3
Per-path AS at BS (Fixed)	2°
BS per-path AoD Distribution	$\eta(0, \sigma^2_{A0D})$ where $\sigma_{AoD} = r_{AS}\sigma_{AS}$
Mean AS and ES at MS	$E(\sigma_{AS,MS}) = 68°$
Per-path AS and ES at MS (fixed)	35°
MS Per-path AoA Distribution	$\eta(0, \sigma^2_{AoA}(PR))$
Delay spread as a log-normal RV $\sigma_{DS} = 10^(\epsilon_{DS}x + \mu_{DS}), x \sim \eta(0,1)$	$\mu_{DS} = -6.18$ $\epsilon_{DS} = 0.18$
Mean total RMS Delay Spread	$E(\sigma_{DS}) = 0.65\mu s$
$r_{DS} = \frac{\sigma_{delays}}{\sigma_{DS}}$	1.7
Log normal shadowing standard deviation, σ_{SF}	8dB
Pathloss model in (dB), d in meters	$34.5 + 35log_{10}(d)$
Tilt Angle	90°

Chapter 4

Results and Discussions

This section provides the outcomes of the MATLAB simulation results of the convergence performance for the correlation and geometry-based stochastic channel models. Analysis is shown for both the URA and CA antenna topology.

4.1 Convergence

From equations (1.6) and (1.7), a convergence channel matrix is defined as $\mathbf{W}$ and this is represented by

$$\mathbf{W} = \frac{1}{M}\mathbf{H}^T\mathbf{H}^* \tag{4.1}$$

In evaluating the convergence, a deviation matrix denoted as $\mathbf{E}$ is defined, which represents the deviation of $\mathbf{W}$ from the identity matrix, $\mathbf{I}$, i.e. $\mathbf{E} = \mathbf{W} - \mathbf{I}$. The Mean Absolute Deviation (MAD) and the Diagonal Dominance (DD) are defined in equation (4.2) and (4.3) as

$$MAD(\mathbf{E}) = \frac{1}{K^2}\sum_{i=1,j=1}^{K} |\mathbf{E}_{ij}| \tag{4.2}$$

$$DD = \frac{\sum_{i=1}^{K} \mathbf{W}_{ii}}{\sum_{i=1}^{K}\sum_{j=1,j\neq i}^{K} |\mathbf{W}_{ij}|} \tag{4.3}$$

Two convergence scenarios are considered. In the first scenario, the number of users, K is kept constant as the transmit antennas, $M \to \infty$ while in the second scenario, K is varied alongside with M. In the performance evaluation, different parameters were varied to investigate its impact on the massive MIMO system convergence. These parameters include;

1. The distance, d_x, referring to the spacing of antenna array elements on the

$x-$plane and d_y, which denotes the spacing of antenna array elements on the $y-$plane.

2. Measure of the spreads of angular distributions of arrival, i.e. the *Standard deviation*, σ (Gaussian), the *decay factor*, α (Laplacian), the *angular spread*, μ (Student's -T) and the *accumulation of the distribution*, κ (Von Misses).

3. The azimuth spread (AS) and the elevation spread (ES) represented as θ and ϕ respectively.

4.2 Convergence Analysis using URA Antenna Topology

4.2.1 Analysis using CBSCM

The Rayleigh fading channel model, ($\mathbf{H} = R_t^{\frac{1}{2}}\mathbf{H}_{iid}$) was used for all the simulations. For the spatial correlation characterization, the SC based on MPA was used. The Mean Absolute Deviation (MAD) and the Diagonal Dominance (DD) was used to evaluate the convergence performance. Each convergence metric is evaluated and averaged over 20 channel realizations. The number of users, K is kept constant at $K = 20$. The azimuth and elevation angles, θ and ϕ respectively is varied between 15° and 60° each. The antenna spacing, d is varied between 0.1λ and 1λ. For the measure of spreads, σ and α are varied between 3 and 10, κ is varied between 4 and 8, and μ is varied between 0.1 and 0.9. Convergence performance is analyzed between the distributions and compared. For the comparison of the spreads angular distributions of arrival and the azimuth and elevation spreads, the correlation factor between the antennas is kept at 0.2λ.

Computing for the Mean Absolute Deviation (MAD)

In Figure 4.1, AS and ES are varied for both Gaussian and Laplacian distributions for M increasing. The two distributions clearly demonstrate that the convergence

increases as M antennas increases. The rate of convergence increases proportionally as the azimuth and elevation angles increases. However, from Figure 4.2, convergence occurs faster for the student t-distribution with higher AS and ES.

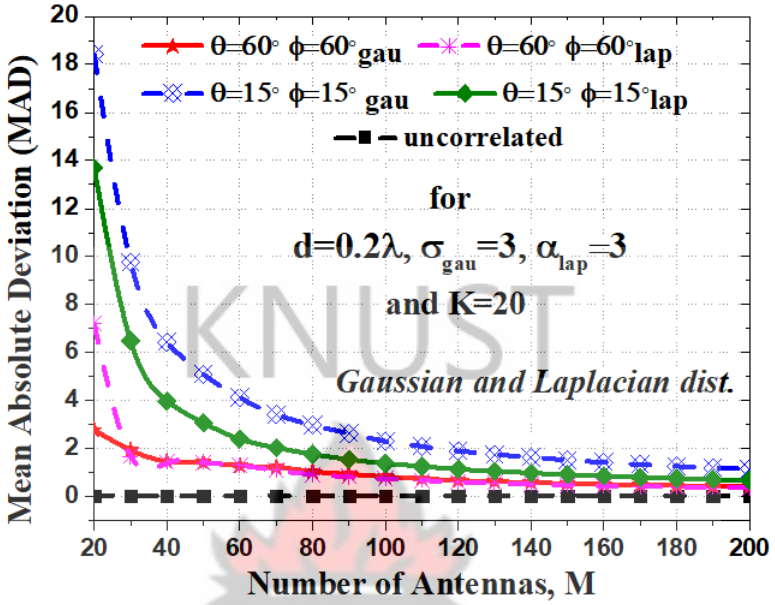

Figure 4.1: Comparing the $MAD(\mathbf{E})$ vs M between gaussian and laplacian distributions with $d = 0.2\lambda, \sigma = 3, \alpha = 3$ and $K = 20$ for varying angles of θ and ϕ.

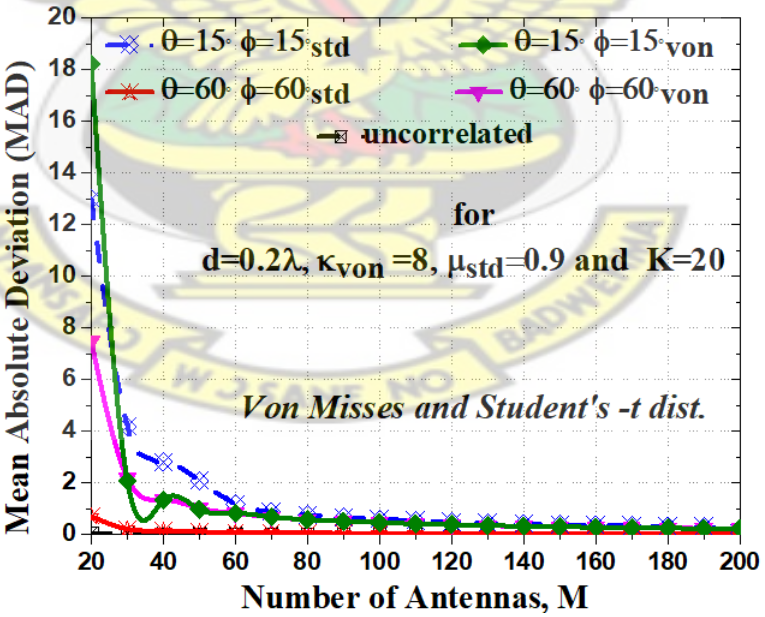

Figure 4.2: Comparing the $MAD(\mathbf{E})$ vs M between von misses and student's -t distributions with $d = 0.2\lambda, \kappa = 8, \mu = 0.9$ and $K = 20$ being fixed for varying angles of θ and ϕ.

From Figures 4.3 and 4.4, it is obvious considering all distributions that the convergence increases proportionally to antenna element spacing, d. This is as a

result of the decrease in the correlation as the distances between antenna elements increases. Also, channel matrices with correlation above 0.5λ showed faster convergence rate. These results therefore supports the existing developments that for massive MIMO channels to be uncorrelated, it requires antenna spacing of at least $\lambda/2$ wavelengths.

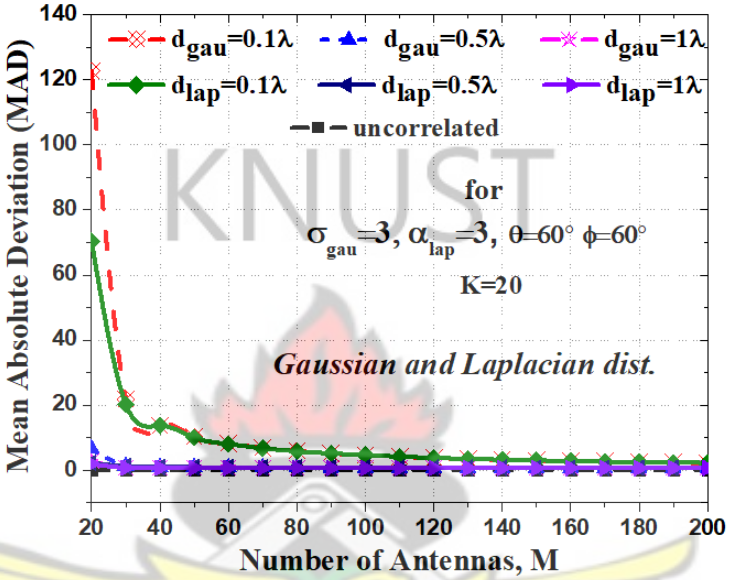

Figure 4.3: Comparing the $MAD(\mathbf{E})$ vs M between gaussian and laplacian distributions for varied antenna element spacing, d with θ and ϕ fixed at 60° each, and $\sigma = 3$ and $\alpha = 3$

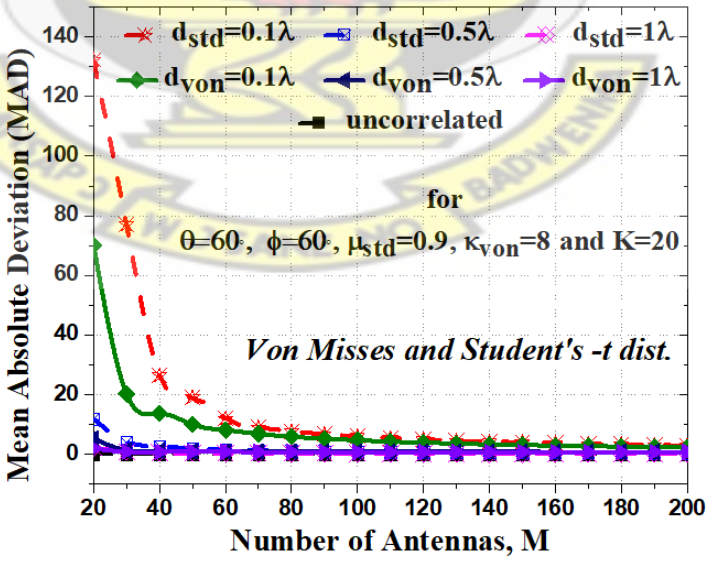

Figure 4.4: Comparing the $MAD(\mathbf{E})$ vs M between von misses and student' t-distributions for varied antenna element spacing, d with θ and ϕ fixed at 60° each, and $\kappa = 8$ and $\mu = 0.9$

Figures 4.5 and 4.6 show the impact of the measures of the spreads i.e. (σ, α, μ and κ) on the convergence. In Figure 4.6, it can be observed that the convergence increases at a rate proportional to the increase in the angular κ and μ. However in Figure 4.5, changing σ and α did not show any sensitivity to the convergence for $M \geq 40$. This occurs due to the decrease in the spatial correlation as the number of antennas increases irrespective of the change in values of σ and α.

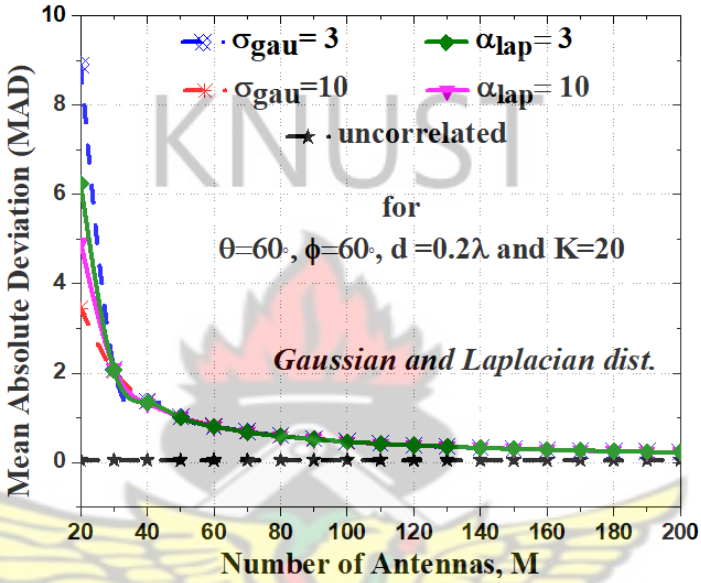

Figure 4.5: Comparing the $MAD(\mathbf{E})$ vs M between gaussian and laplacian distributions for angular spreads, σ and α with θ and ϕ fixed at 60° each, and $d = 0.2\lambda$

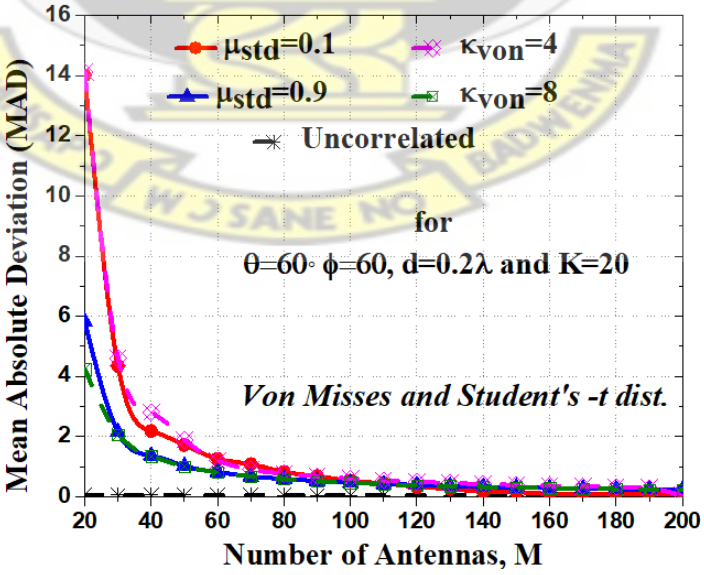

Figure 4.6: Comparing the $MAD(\mathbf{E})$ vs M between von missess and student's t-distributions for angular spreads, κ and μ with θ and ϕ fixed at 60° each, and $d = 0.2\lambda$

Computing for Diagonal Dominance

Figures 4.7 - 4.12 illustrates the Diagonal Dominance of $\mathbf{W}$ as M grow large. The number of users is set at $K = 10$. While for an i.i.d. or uncorrelated channel where $\mathbf{W}$ becomes increasingly diagonal as the sum of elements in the diagonal grow faster than the fixed number of elements in the off-diagonals, the diagonal dominance converges quickly to zero for the correlated channels as M increases. Figures 4.7 and 4.8 show a change in the rate of change in the convergence as the elevation and azimuth angles vary. A similar trend is realized in varying antenna element spacing as depicted in Figures 4.9 and 4.10 and also that of varying spreads of the distribution as illustrated in Figures 4.11 and 4.12.

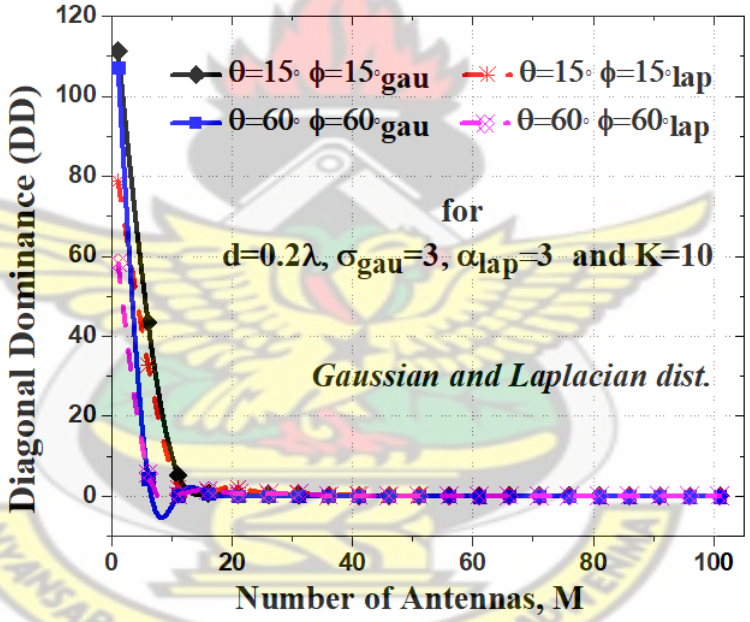

Figure 4.7: Comparing the DD vs M between gaussian and laplacian distributions with $d = 0.2\lambda, \sigma = 3, \alpha = 3$ for varying angles of θ and ϕ.

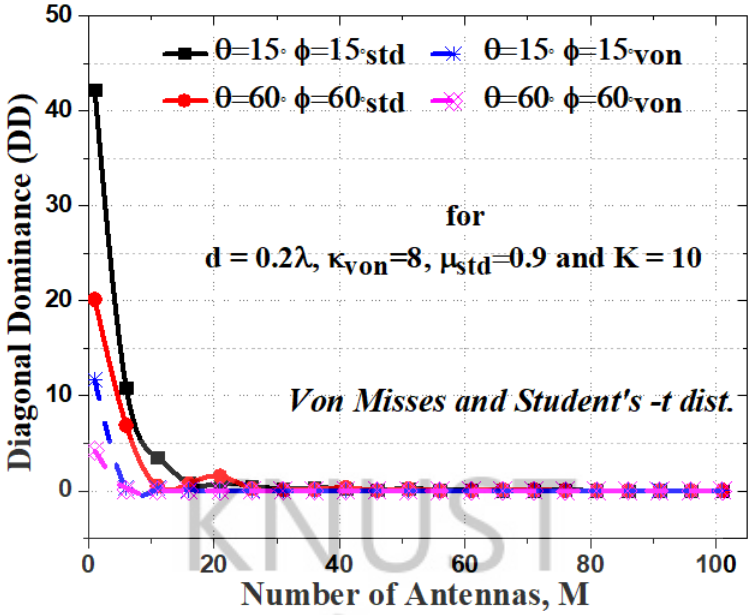

Figure 4.8: Comparing the DD vs M between von misses and student's -t distributions with $d = 0.2\lambda, \kappa = 8, \mu = 0.9$ for varying angles of θ and ϕ.

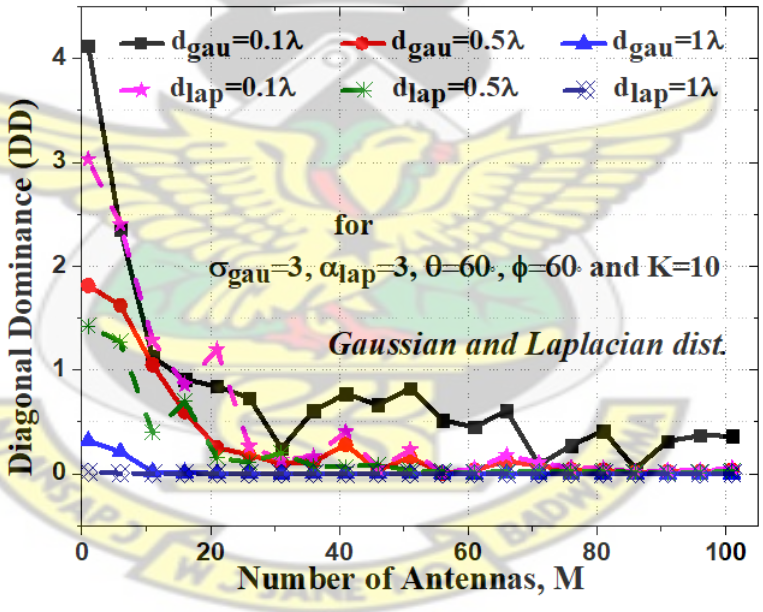

Figure 4.9: Comparing the DD vs M between gaussian and laplacian distributions for varied antenna element spacing, d with θ and ϕ fixed at 60° each, and $\sigma = 3$ and $\alpha = 3$

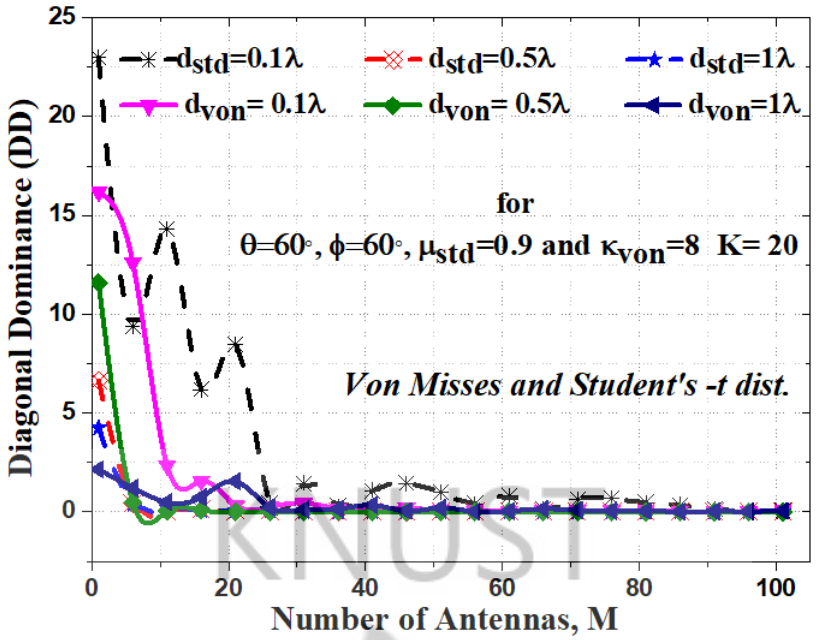

Figure 4.10: Comparing the DD vs M between von misses and student' t-distributions for varied antenna element spacing, d with θ and ϕ fixed at 60° each, and $\kappa = 8$ and $\mu = 0.9$

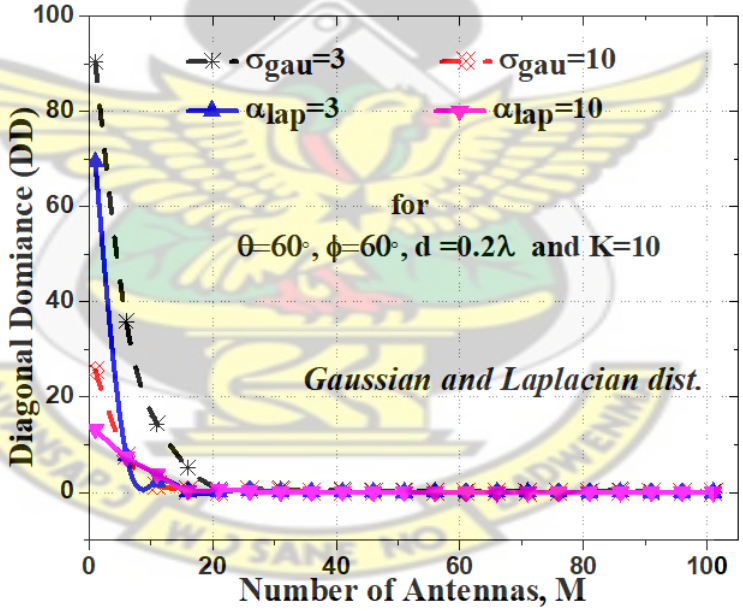

Figure 4.11: Comparing the DD vs M between gaussian and laplacian distributions for angular spreads, σ and α with θ and ϕ fixed at 60° each, and $d = 0.2\lambda$

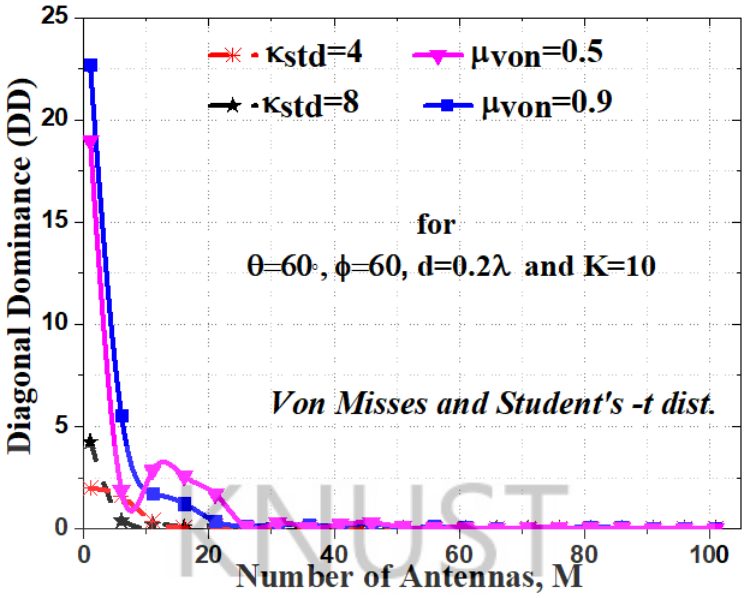

Figure 4.12: Comparing the DD vs M between von missess and student's t-distributions for angular spreads, κ and μ with θ and ϕ fixed at 60° each, and $d = 0.2\lambda$

In summary, the simulation results demonstrated that the increase in the elevation and azimuth angles both contributed to increase of the convergence performance in the correlation-based channel model. The convergence also showed better performance for antenna spacing of 0.5λ for all the different distributions.

4.2.2 Analysis using GBSCM

In this section, the 3D channel matrix, $[\mathbf{H}_{s,u}]$ which reflects practical massive MIMO system analysis is used for all the simulations. Each convergence metric is evaluated and averaged over 10 channel realizations.

Just as in the case of the CBSCM, the number of users, K is kept constant at $K = 20$. The azimuth and elevation angles, θ and ϕ respectively, is varied between 15° and 60° each. The antenna spacing, d is varied between 0.1λ and 1λ. For the measure of spreads, σ and α are varied between 3 and 10, κ is varied between 4 and 8, and μ is varied between 0.1 and 0.9.

Computing for the Mean Absolute Deviation (MAD)

In computing the Mean Absolute deviation of $[\mathbf{H}_{s,u}]$ from $\mathbf{I}$, the simulation results of the 3D geometry-based channel demonstrates that the convergence increases at a rate proportional to the azimuth and elevation angles, the antenna element spacing and the angular spreads of distributions for Student's t and Gaussian distributions as depicted in Figures 4.13 - 4.18. However, the Laplacian and Von Misses distributions showed poor convergence performance, even for AS and ES increasing with increasing spreads of the distributions. The poor performance of the Laplacian and Von Misses distribution was due to the high values of spatial correlation coefficients registered, as the number of antenna elements increased.

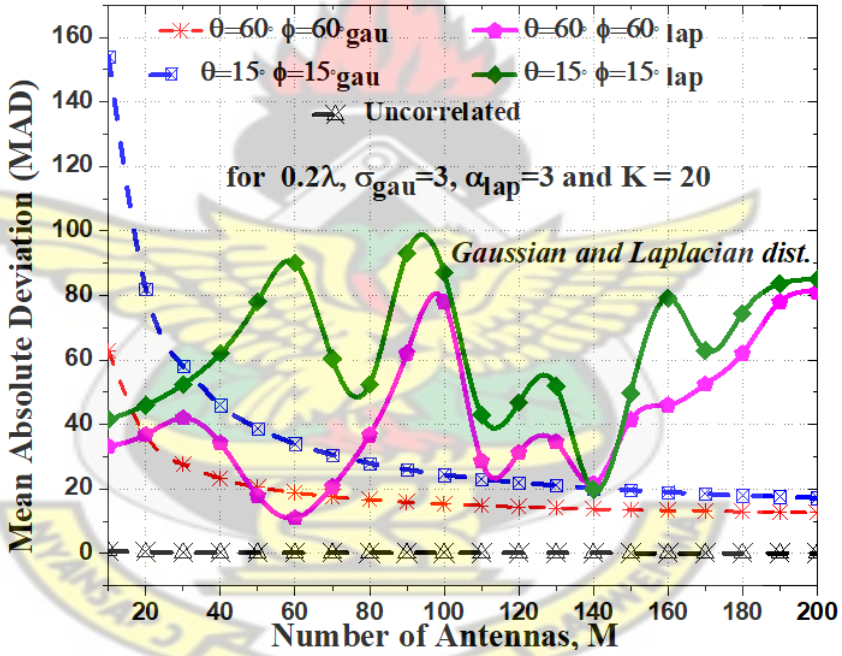

Figure 4.13: Comparing the $MAD(\mathbf{E})$ vs M between gaussian and laplacian distributions with $d = 0.2\lambda, \sigma = 3, \alpha = 3$ for varying angles of θ and ϕ.

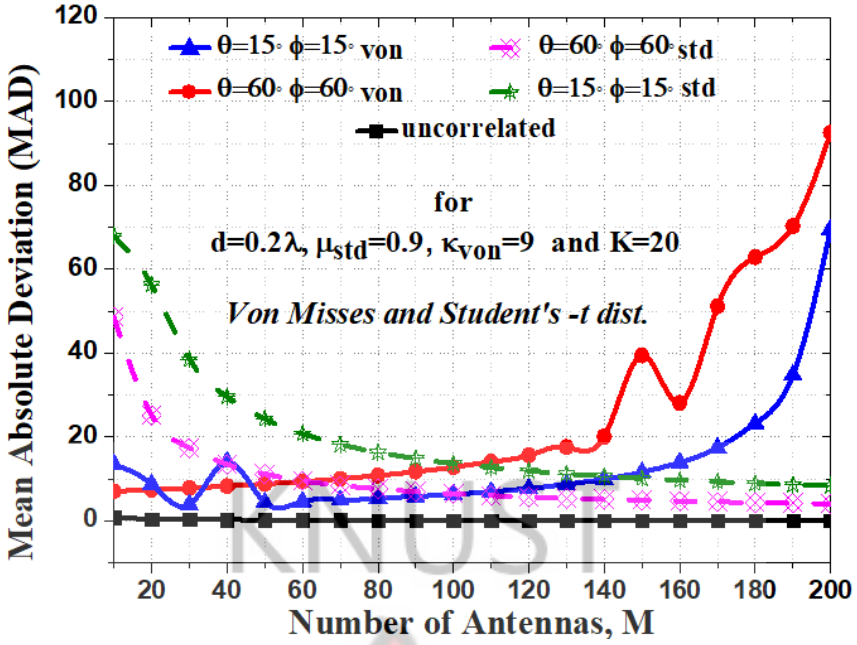

Figure 4.14: Comparing the $MAD(\mathbf{E})$ vs M between von misses and student's -t distributions with $d = 0.2\lambda, \kappa = 8, \mu = 0.9$ for varying angles of θ and ϕ.

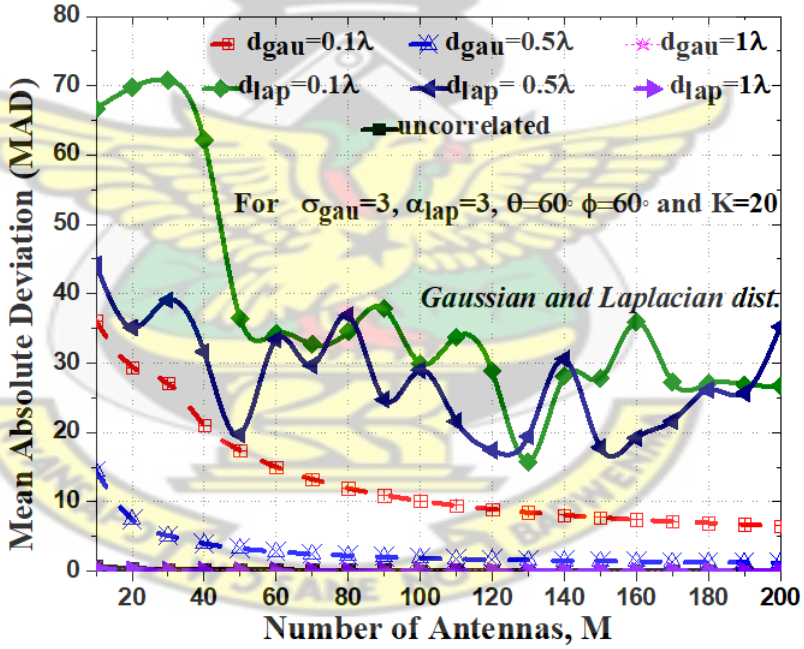

Figure 4.15: Comparing the $MAD(\mathbf{E})$ vs M between gaussian and laplacian distributions for varied antenna element spacing, d with θ and ϕ fixed at 60° each, and $\sigma = 3$ and $\alpha = 3$

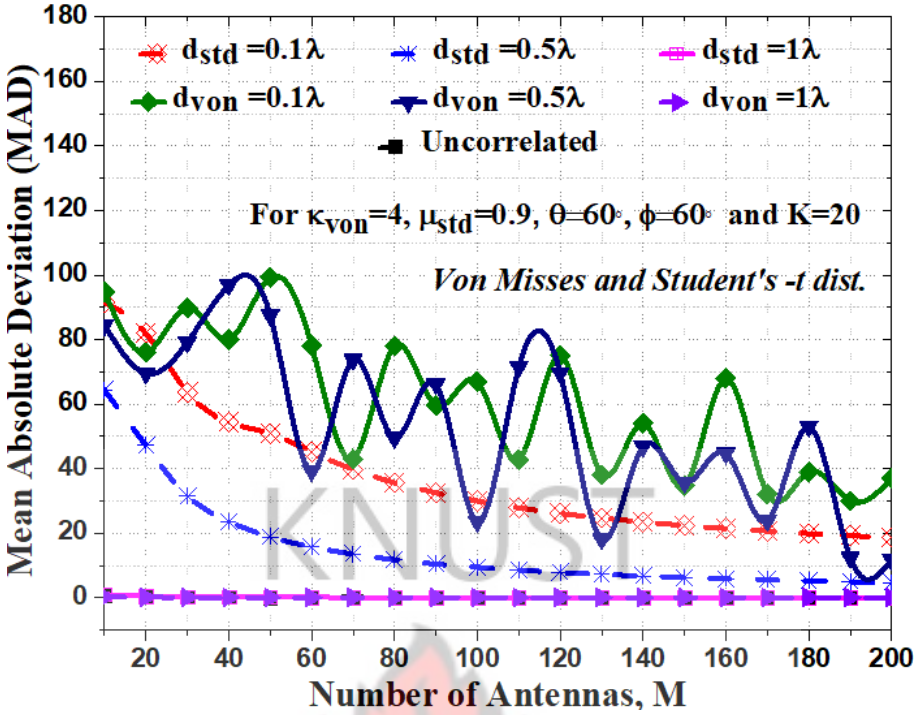

Figure 4.16: Comparing the $MAD(\mathbf{E})$ vs M between von misses and student' t-distributions for varied antenna element spacing, d with θ and ϕ fixed at 60° each, and $\kappa = 8$ and $\mu = 0.9$

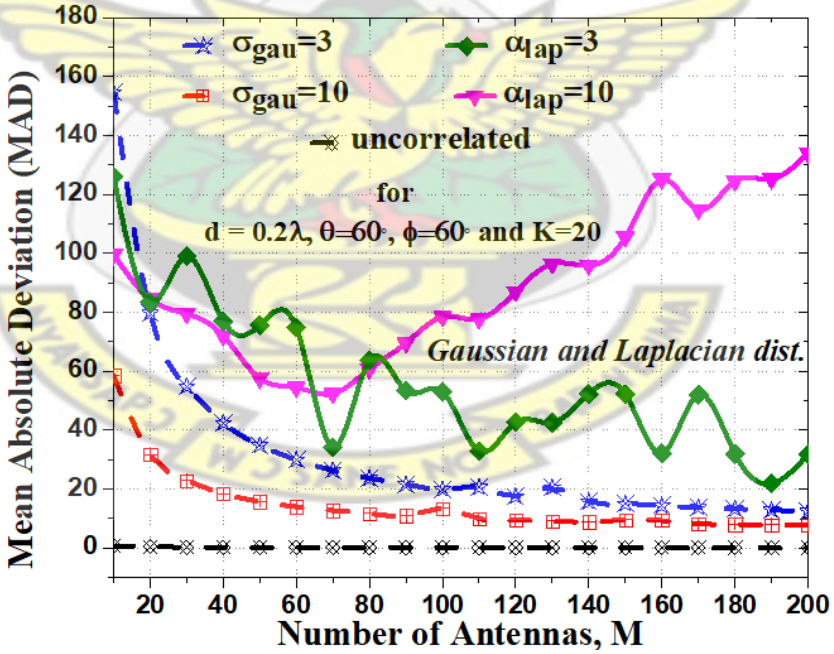

Figure 4.17: Comparing the $MAD(\mathbf{E})$ vs M between gaussian and laplacian distributions for angular spreads, σ and α with θ and ϕ fixed at 60° each, and $d = 0.2\lambda$

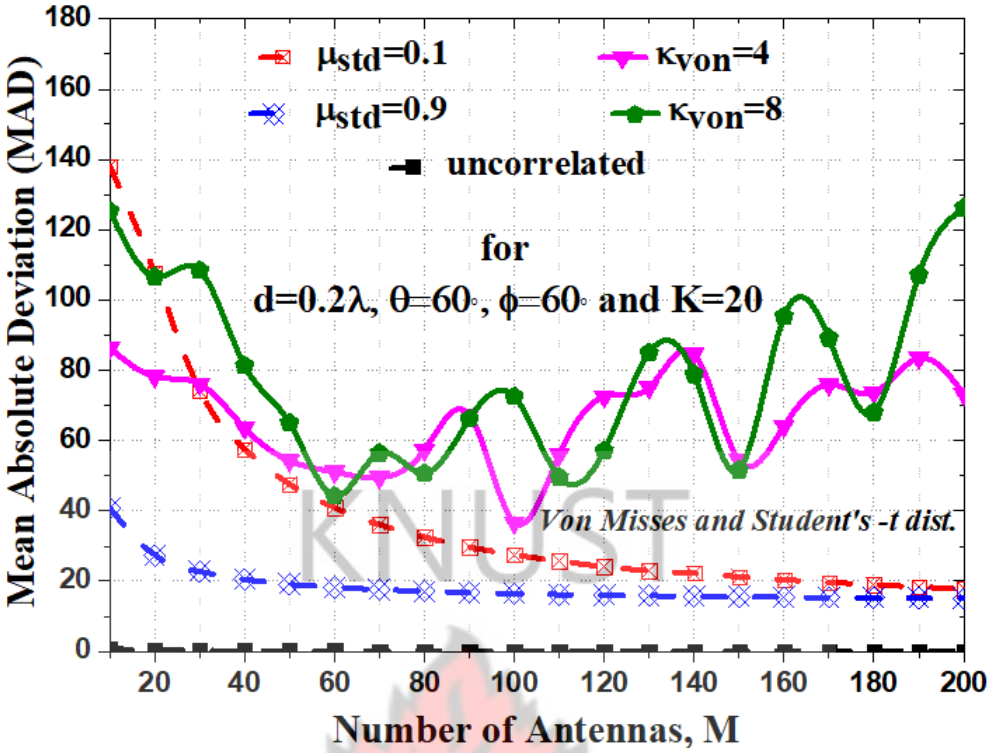

Figure 4.18: Comparing the $MAD(\mathbf{E})$ vs M between von missess and student's t-distributions for angular spreads, κ and μ with θ and ϕ fixed at 60° each, and $d = 0.2\lambda$

Computing for the Diagonal Dominance (DD)

Unlike in the case of the CBSCM, the diagonal dominance becomes increasingly diagonal with K being fixed as M grows large. From Figures 4.19 - 4.24, the diagonal dominance deteriorates proportionally to the azimuth and elevation angles, angular spreads and the antenna spacing for Gaussian and Student's -t distributions. The diagonal dominance however converges to zero quickly as M increases for the Laplacian and Von Misses distributions.

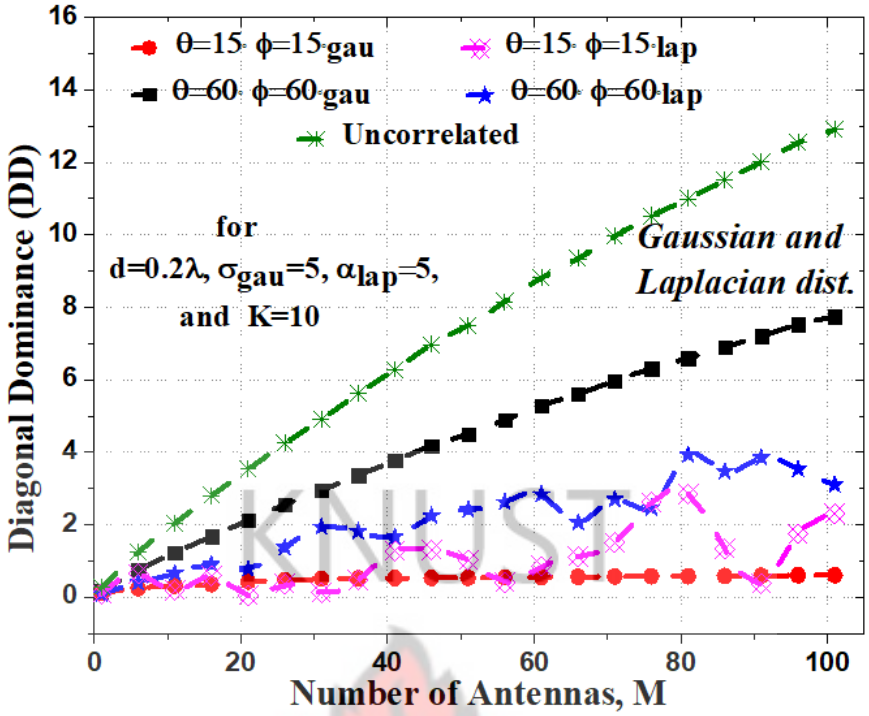

Figure 4.19: Comparing the DD vs M between gaussian and laplacian distributions with $d = 0.2\lambda, \sigma = 3, \alpha = 3$ and $K = 20$ for varying angles of θ and ϕ.

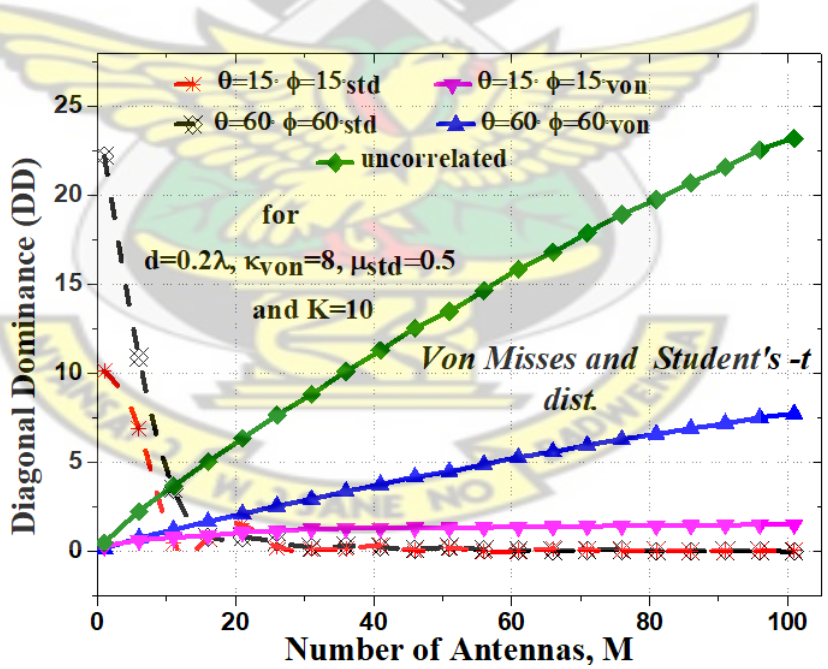

Figure 4.20: Comparing the DD vs M between von misses and student's -t distributions with $d = 0.2\lambda, \kappa = 8, \mu = 0.9$ and $K = 20$ being fixed for varying angles of θ and ϕ.

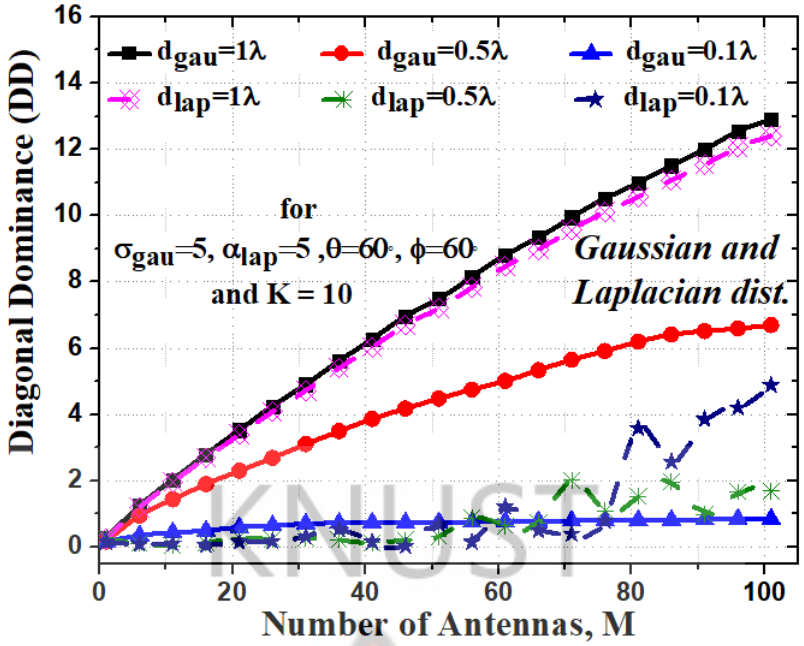

Figure 4.21: Comparing the DD vs M between gaussian and laplacian distributions for varied antenna element spacing, d with θ and ϕ fixed at 60° each, and $\sigma = 3$ and $\alpha = 3$

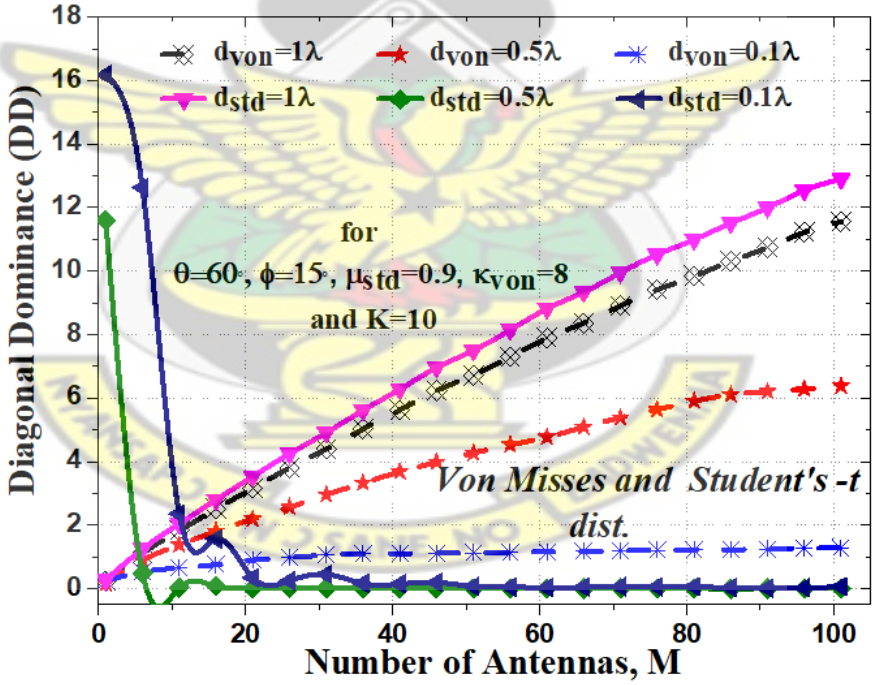

Figure 4.22: Comparing the DD vs M between von misses and student' t-distributions for varied antenna element spacing, d with θ and ϕ fixed at 60° each, and $\kappa = 8$ and $\mu = 0.9$

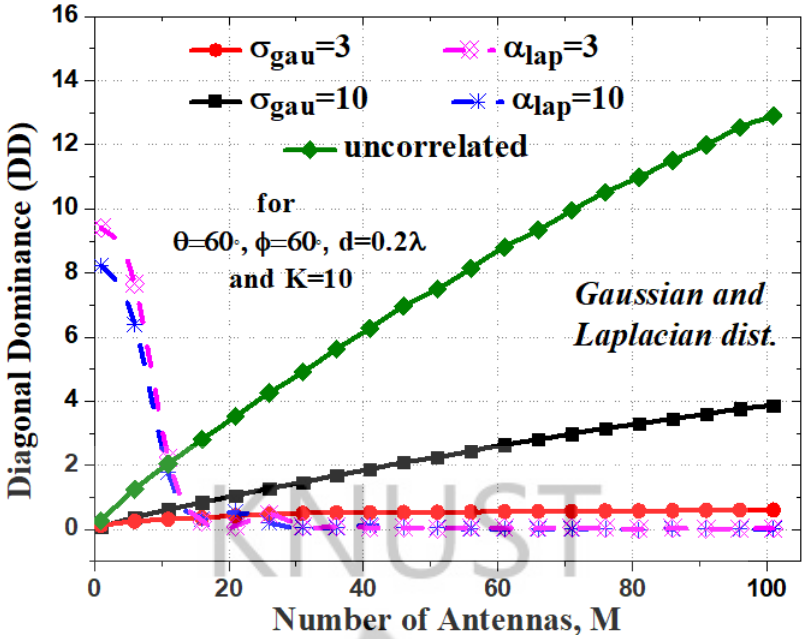

Figure 4.23: Comparing the DD vs M between gaussian and laplacian distributions for angular spreads, σ and α with θ and ϕ fixed at 60° each, and $d = 0.2\lambda$

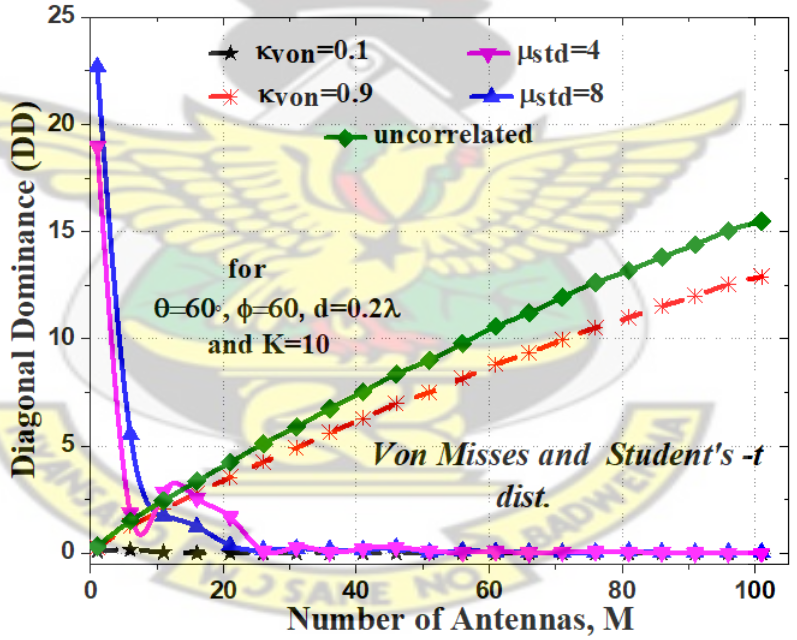

Figure 4.24: Comparing the DD vs M between von missess and student's t-distributions for angular spreads, κ and μ with θ and ϕ fixed at 60° each, and $d = 0.2\lambda$

Computing for MAD as both K and M increases

In this section, the number of users K is made to increase as M also grow large. From Figures 4.25 - 4.26, it was observed that as K approaches closely to M, the convergence performance deviates, for smaller antenna spacing, d. However,

the convergence is better as the antenna spacing increases (i.e. $\lambda/2$ wavelengths), even while K approaches M closely. This is realized for the different angular distributions.

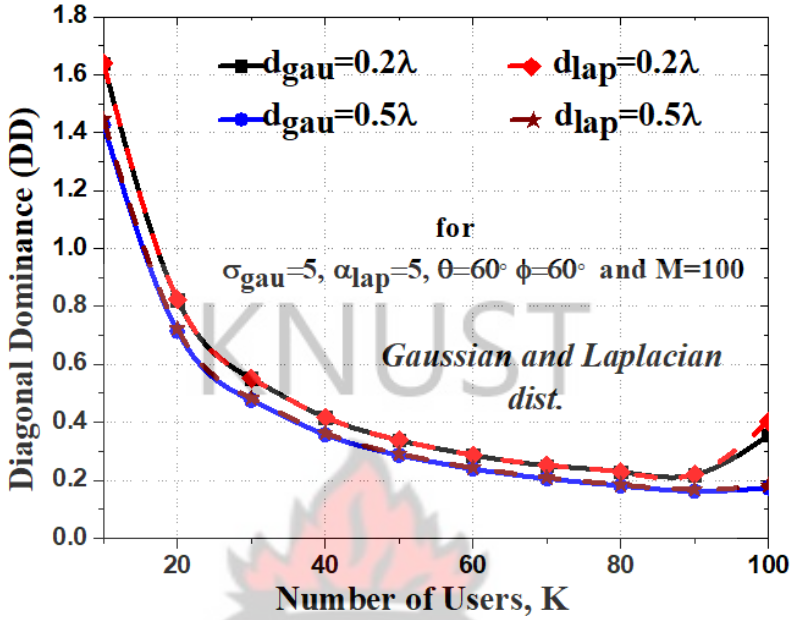

Figure 4.25: MAD vs M for K increasing with α and σ remaining constant whilst varying the θ and ϕ.

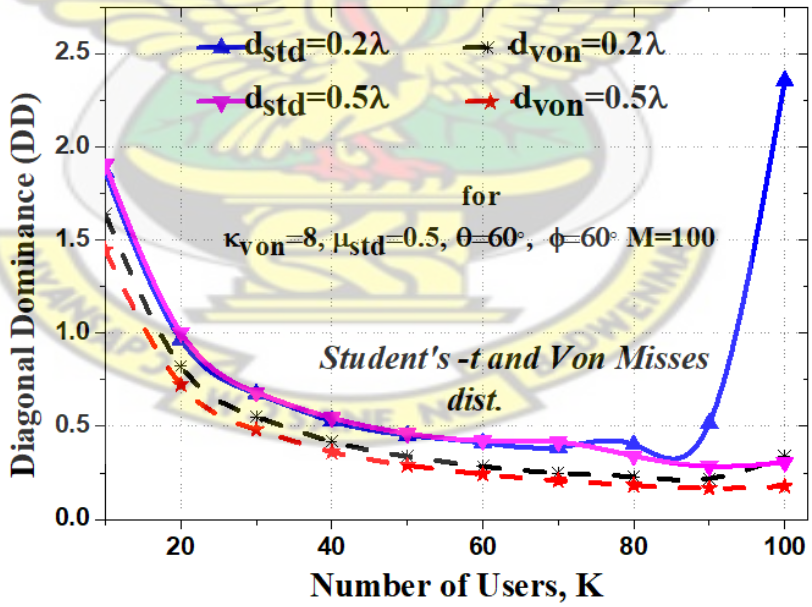

Figure 4.26: MAD vs M for K increasing with κ, μ, θ and ϕ remaining constant whilst varying the antenna element spacing, d.

In Analyzing the simulation results of the convergence for the URA topology, it is realized that the channel begins to exhibit convergence for antenna numbers, M in excess of more than 200 antennas. Results for the Laplacian and Von

Misses distributions however do not show good performances for the analysis of the convergence in the geometry-based channel model.

4.3 Convergence Analysis Using CA Antenna Topology

This section presents the simulation results for CA antenna topology.

4.3.1 Analysis using CBSCM

Just as was presented for the case of the URA antenna topology, the same analysis is done for the case of the CA antenna topology.

Computing for the Mean Absolute Deviation (MAD)

Unlike the URA antenna topology where the channel began to show convergence for antenna numbers in excess of about 200, in the case of the CA antenna topology, the system begins to exhibit convergence at $M \geq 100$. In Figures 4.27 - 4.32, the results support the existing development that the convergence increases proportionally to the spreads of the angular distributions, the antenna element spacing and the azimuth and elevation angles (ES and AS respectively).

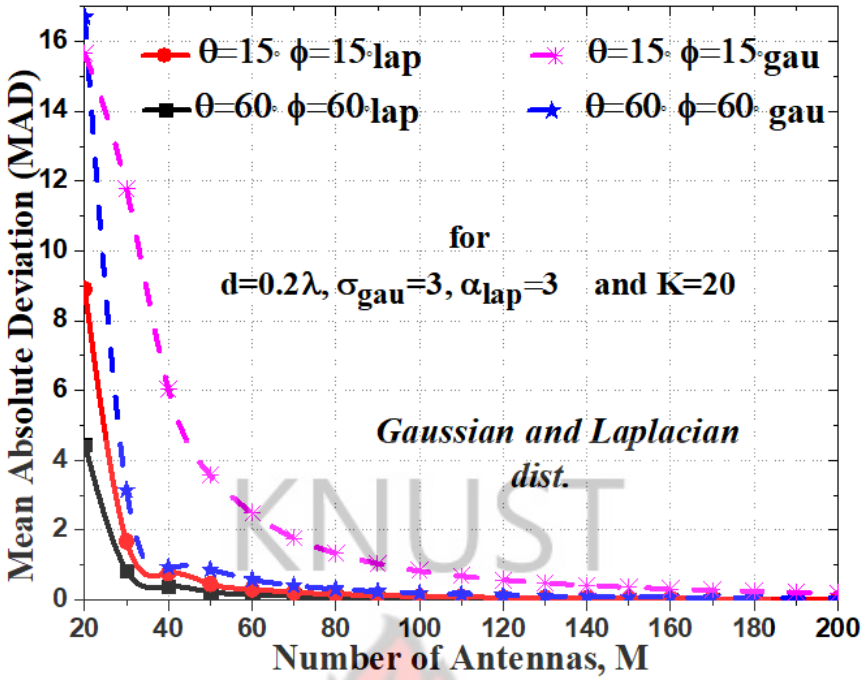

Figure 4.27: Comparing the $MAD(\mathbf{E})$ vs M between gaussian and laplacian distributions with $d = 0.2\lambda, \sigma = 3, \alpha = 3$ and $K = 20$ for varying angles of θ and ϕ.

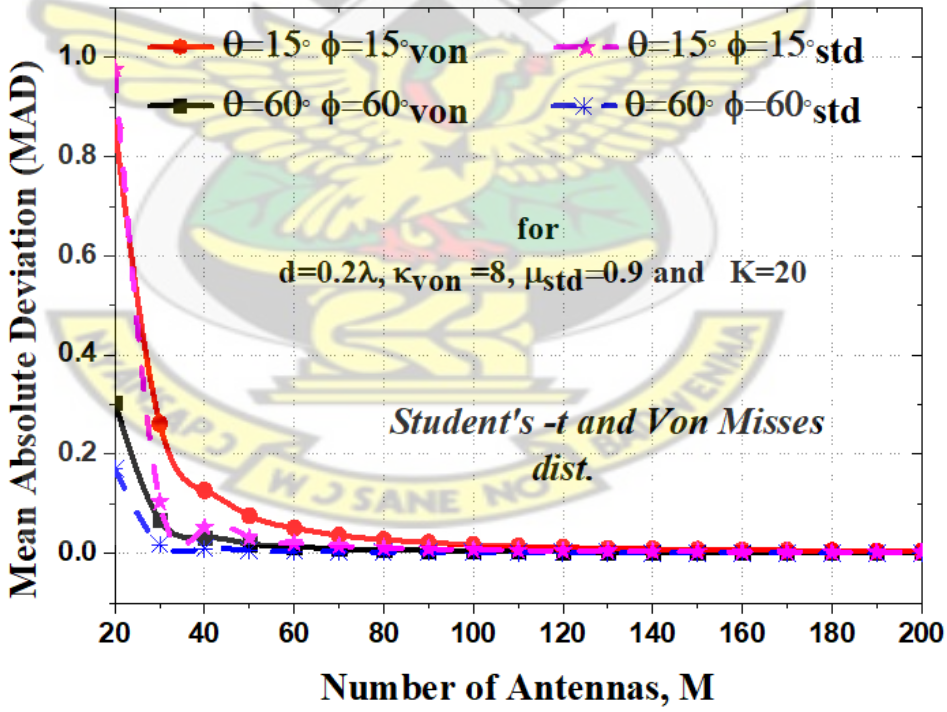

Figure 4.28: Comparing the $MAD(\mathbf{E})$ vs M between von misses and student's -t distributions with $d = 0.2\lambda, \kappa = 8, \mu = 0.9$ and $K = 20$ being fixed for varying angles of θ and ϕ.

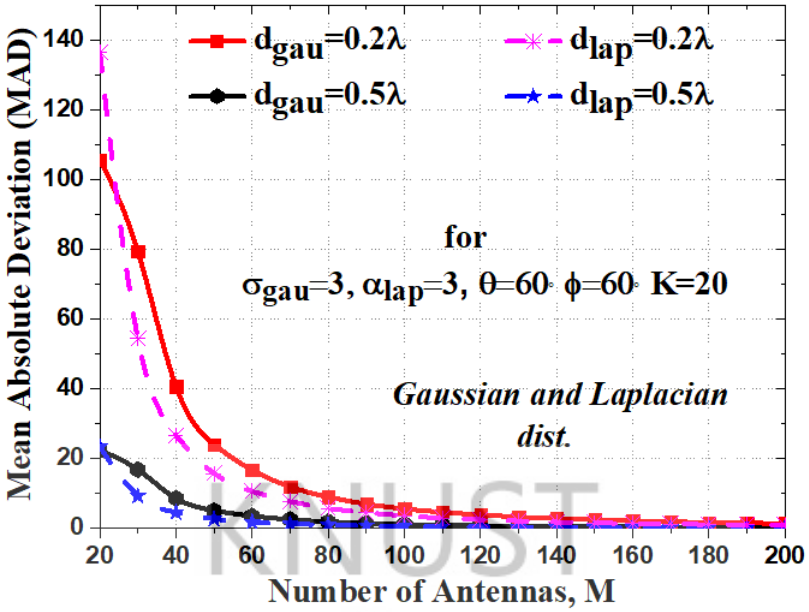

Figure 4.29: Comparing the $MAD(\mathbf{E})$ vs M between gaussian and laplacian distributions for varied antenna element spacing, d with θ and ϕ fixed at 60° each, and $\sigma = 3$ and $\alpha = 3$

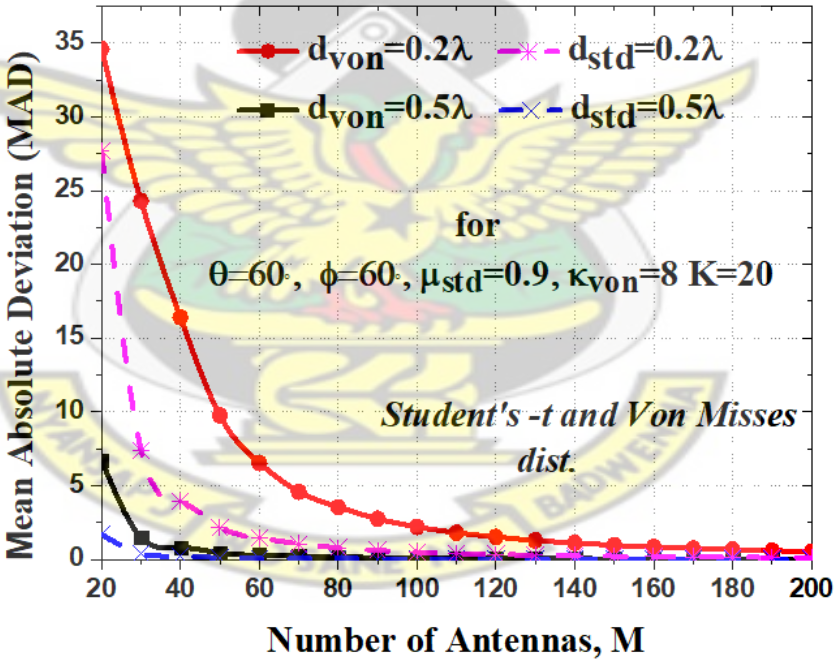

Figure 4.30: Comparing the $MAD(\mathbf{E})$ vs M between von misses and student' t-distributions for varied antenna element spacing, d with θ and ϕ fixed at 60° each, and $\kappa = 8$ and $\mu = 0.9$

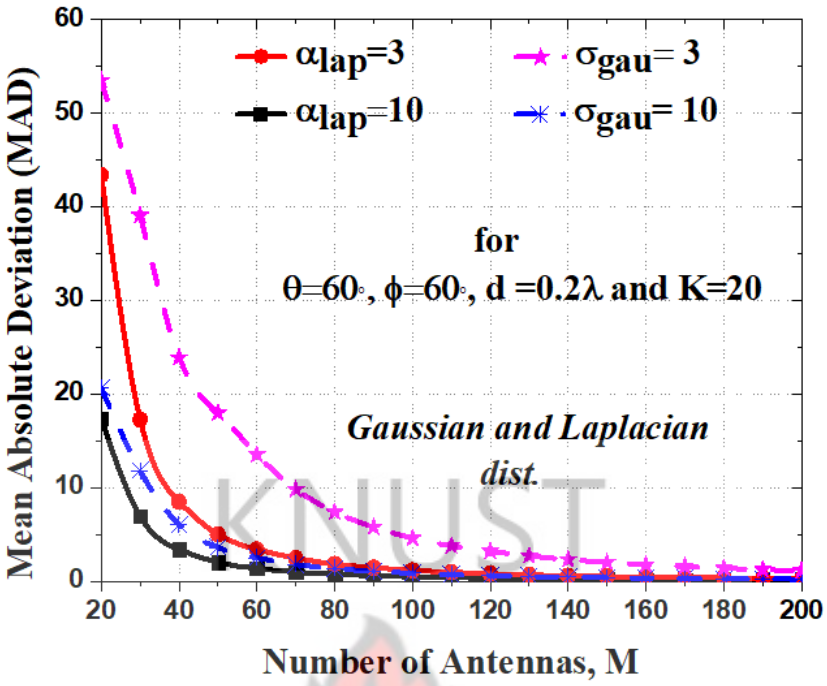

Figure 4.31: Comparing the $MAD(\mathbf{E})$ vs M between gaussian and laplacian distributions for angular spreads, σ and α with θ and ϕ fixed at 60° each, and $d = 0.2\lambda$

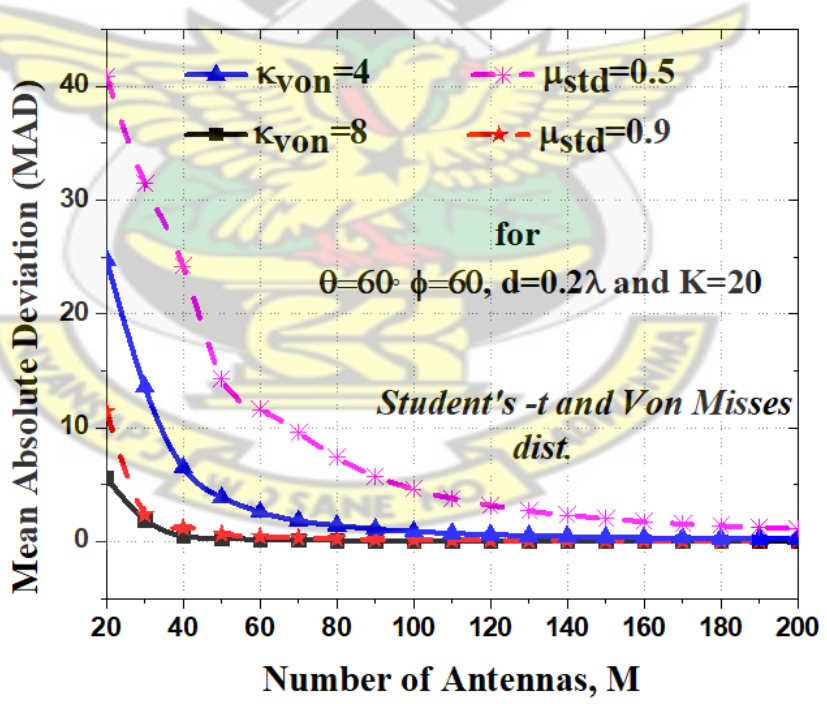

Figure 4.32: Comparing the $MAD(\mathbf{E})$ vs M between von missess and student's t-distributions for angular spreads, κ and μ with θ and ϕ fixed at 60° each, and $d = 0.2\lambda$

Computing for the Diagonal Dominance (DD)

In the case of the diagonal dominance, the convergence channel quickly converges to small non-zero values as a result of the correlation. From Figures 4.33 - 4.38, it can be seen that the channel showed different performance for varying θ and ϕ, d and the angular spreads of the angular distributions. This is due to the fact that θ, ϕ, d and the spreads of the distributions are all functions of the spatial correlation. Therefore, change in these parameters influence the spatial correlation of the massive MIMO channel which in turn affects the convergence.

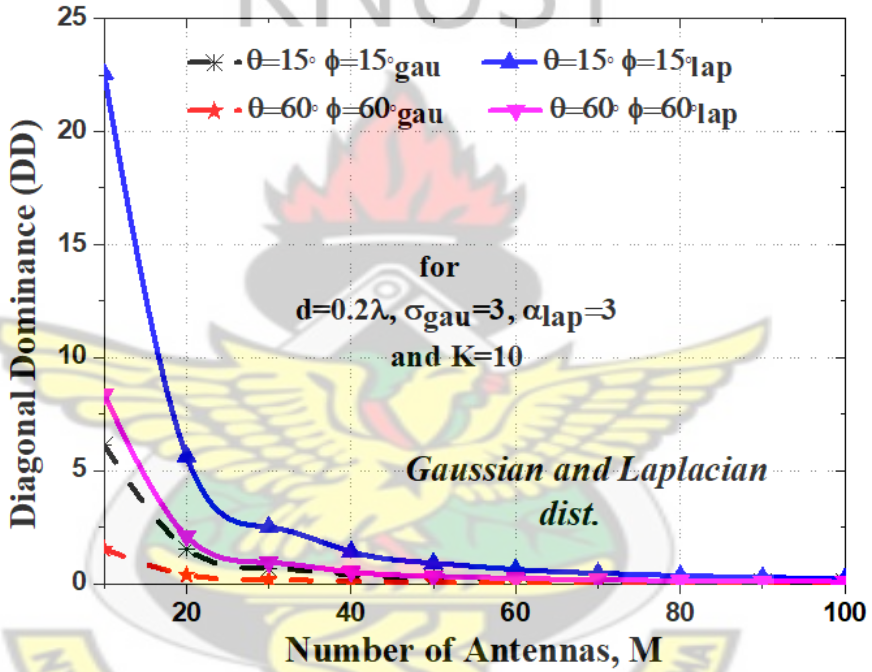

Figure 4.33: Comparing the DD vs M between gaussian and laplacian distributions with $d = 0.2\lambda, \sigma = 3, \alpha = 3$ for varying angles of θ and ϕ.

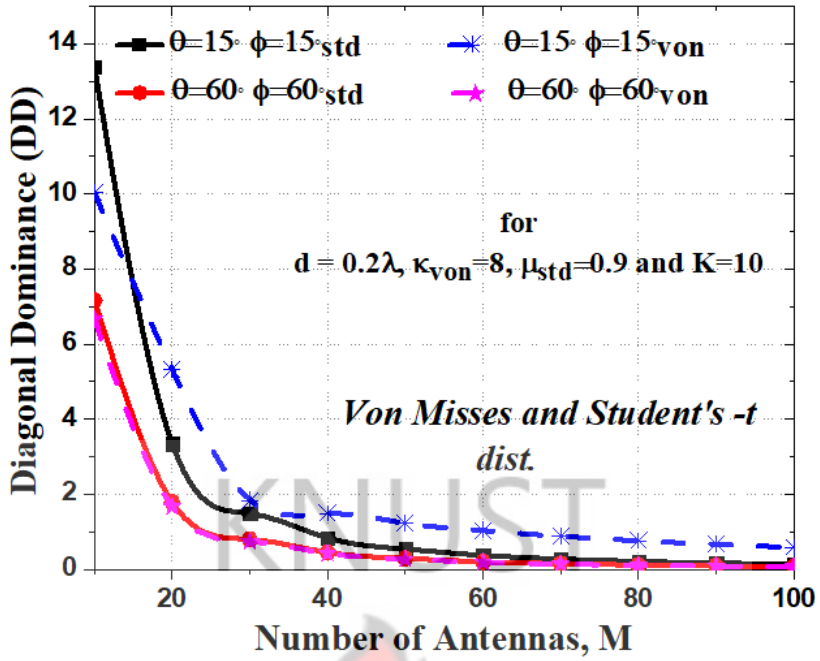

Figure 4.34: Comparing the DD vs M between von misses and student's -t distributions with $d = 0.2\lambda, \kappa = 8, \mu = 0.9$ for varying angles of θ and ϕ.

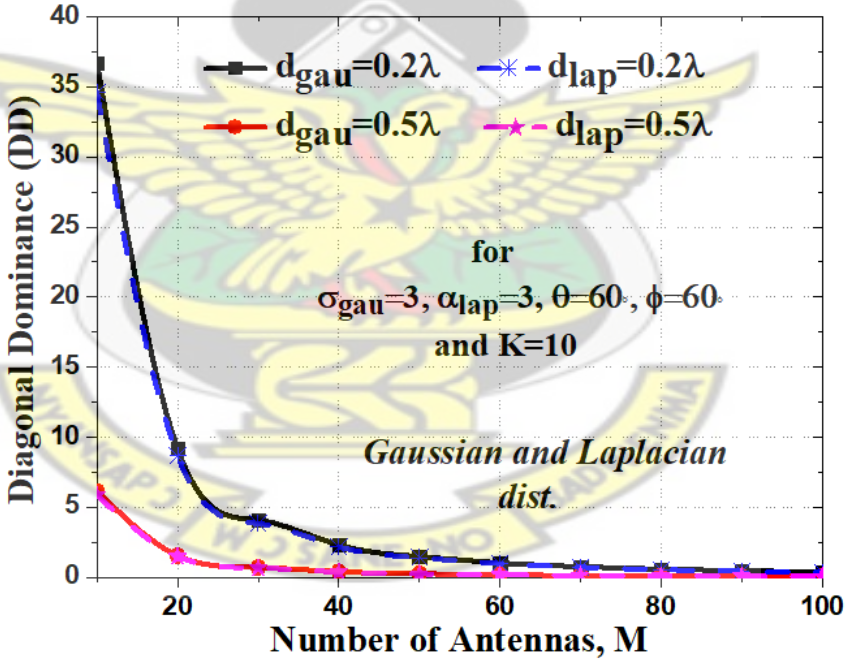

Figure 4.35: Comparing the DD vs M between gaussian and laplacian distributions for varied antenna element spacing, d with θ and ϕ fixed at 60° each, and $\sigma = 3$ and $\alpha = 3$

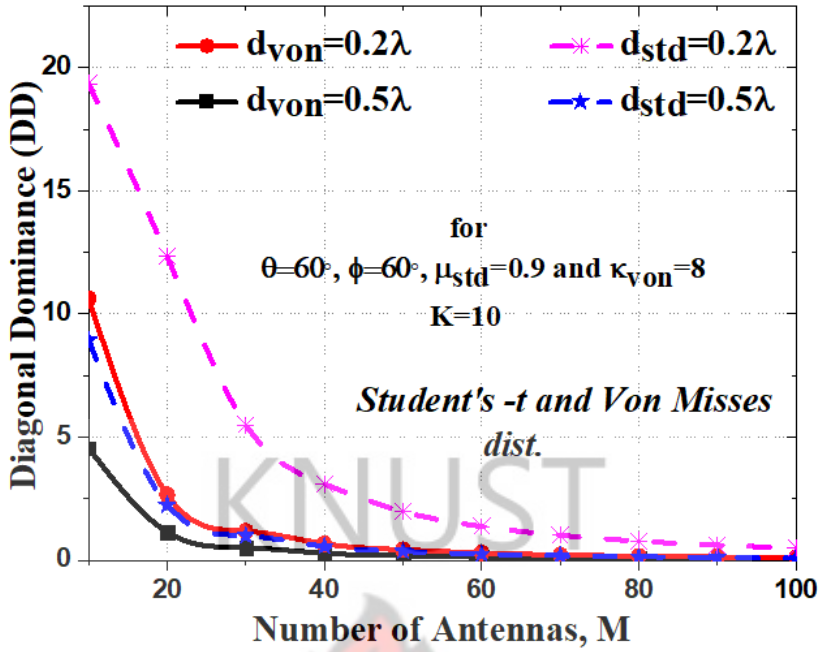

Figure 4.36: Comparing the DD vs M between von misses and student' t-distributions for varied antenna element spacing, d with θ and ϕ fixed at 60° each, and $\kappa = 8$ and $\mu = 0.9$

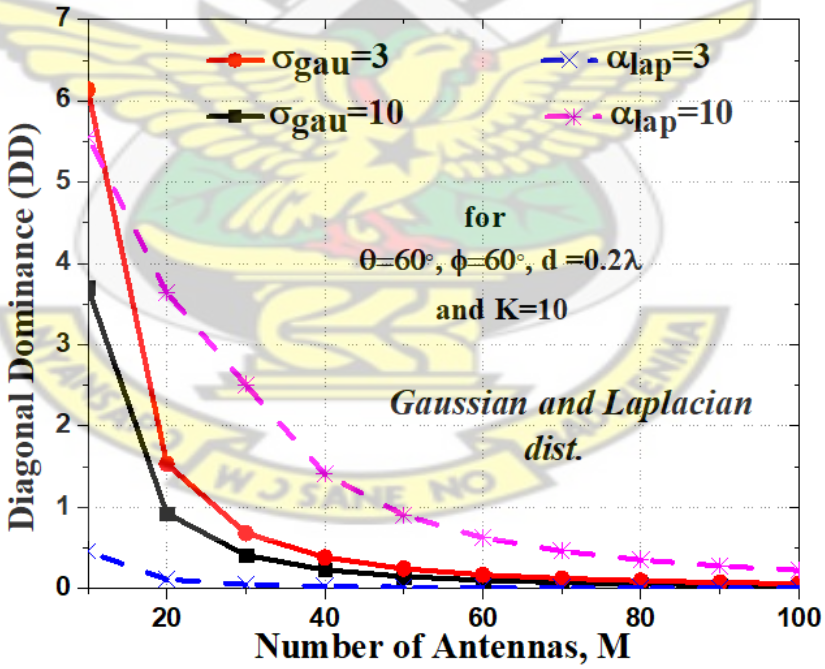

Figure 4.37: Comparing the DD vs M between gaussian and laplacian distributions for angular spreads, σ and α with θ and ϕ fixed at 60° each, and $d = 0.2\lambda$

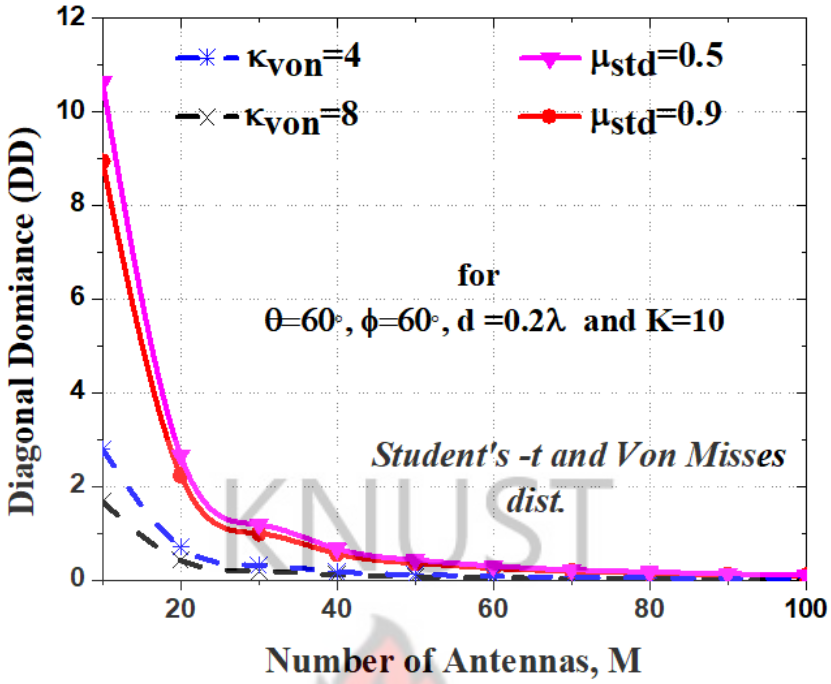

Figure 4.38: Comparing the $DD(\mathbf{E})$ vs M between von missess and student's t-distributions for angular spreads, κ and μ with θ and ϕ fixed at 60° each, and $d = 0.2\lambda$

4.3.2 Analysis using GBSCM

As was done for the case of the URA antenna topology, the 3D channel matrix, $[\mathbf{H}_{s,u}]$ which reflects practical massive MIMO system analysis is used for all the simulations for this section.

Computing for the Mean Absolute Deviation (MAD)

In the analysis of the MAD for the GBSCM channel models, the channel convergence occurs for $M \geq 60$. From the results, it can be observed for most cases that the change in d, θ, ϕ and the spreads of the angular distributions (σ, κ, μ and α) does not show sensitivity to the convergence for approximately $M \geq 80$.

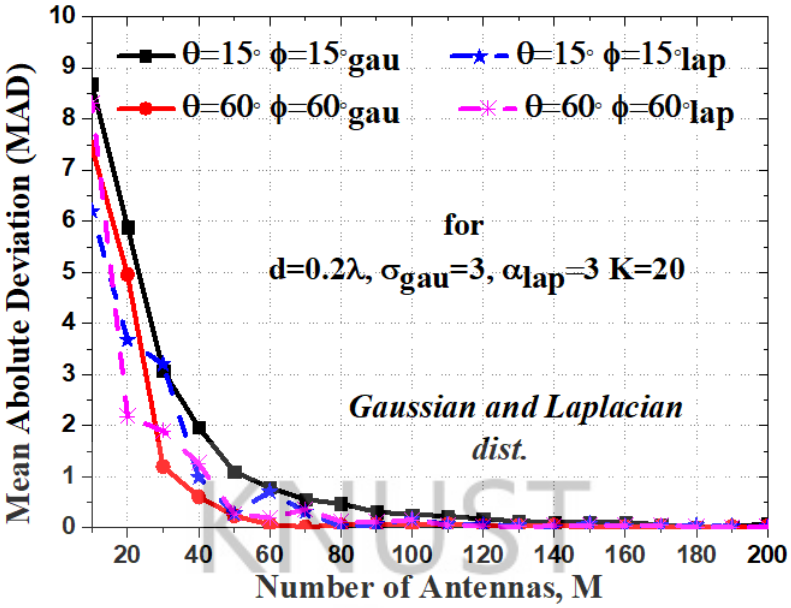

Figure 4.39: Comparing the $MAD(\mathbf{E})$ vs M between gaussian and laplacian distributions with $d = 0.2\lambda, \sigma = 3, \alpha = 3$ and $K = 20$ for varying angles of θ and ϕ.

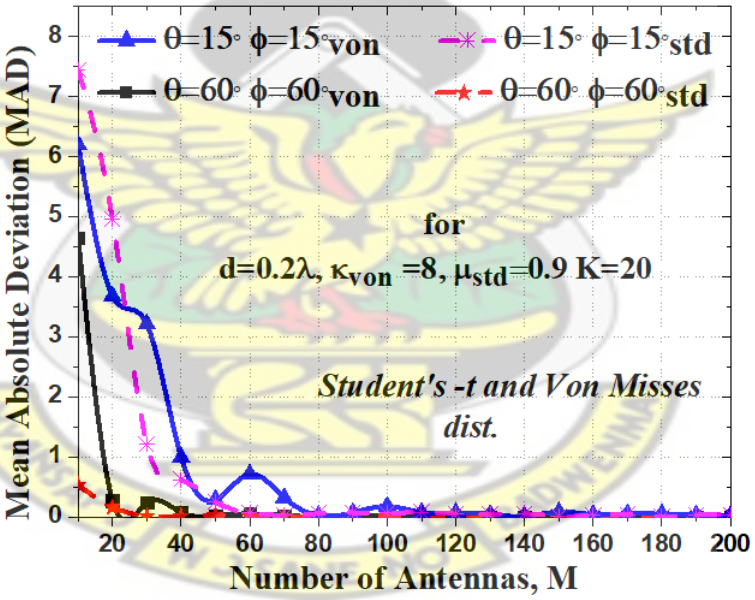

Figure 4.40: Comparing the $MAD(\mathbf{E})$ vs M between von misses and student's -t distributions with $d = 0.2\lambda, \kappa = 8, \mu = 0.9$ and $K = 20$ being fixed for varying angles of θ and ϕ.

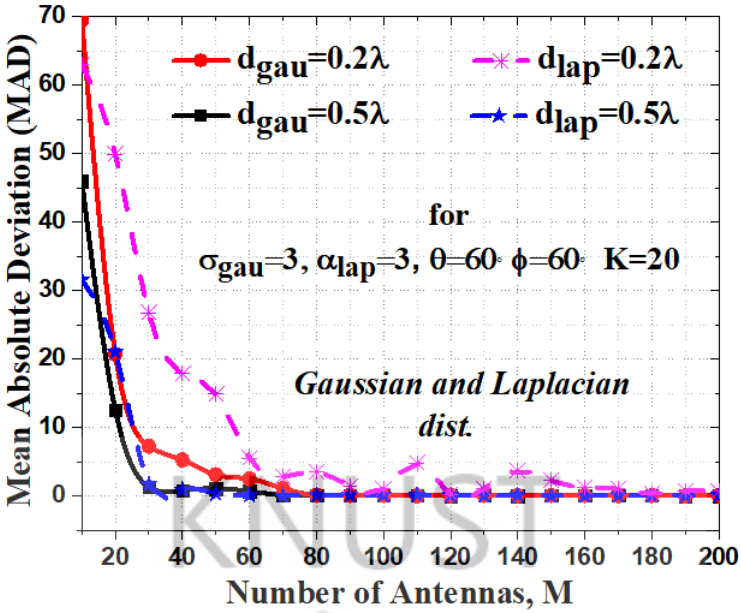

Figure 4.41: Comparing the $MAD(\mathbf{E})$ vs M between gaussian and laplacian distributions for varied antenna element spacing, d with θ and ϕ fixed at 60° each, and $\sigma = 3$ and $\alpha = 3$

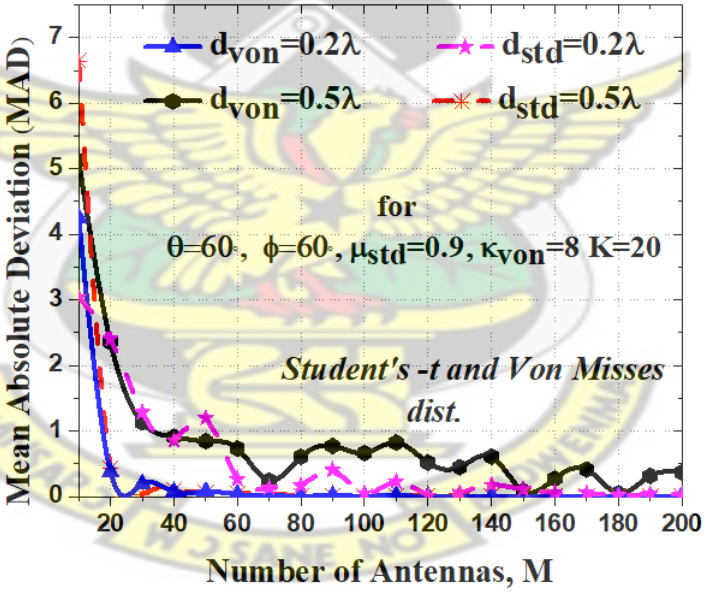

Figure 4.42: Comparing the $MAD(\mathbf{E})$ vs M between von misses and student' t-distributions for varied antenna element spacing, d with θ and ϕ fixed at 60° each, and $\kappa = 8$ and $\mu = 0.9$

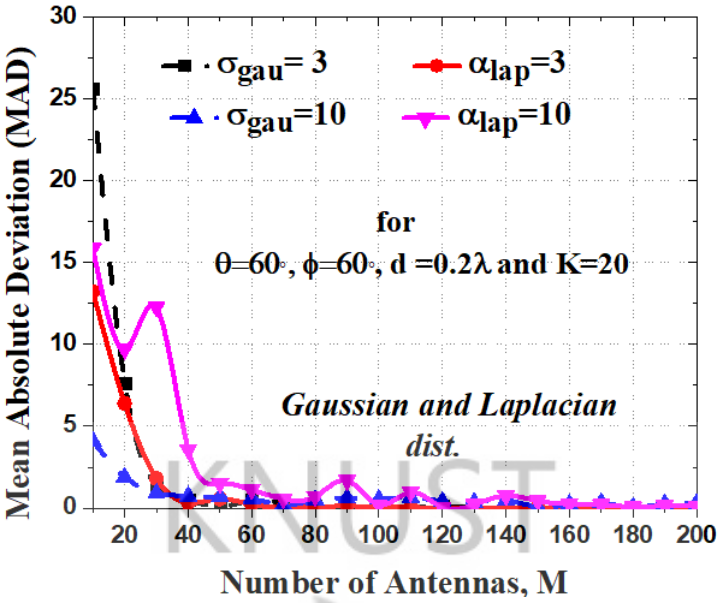

Figure 4.43: Comparing the $MAD(\mathbf{E})$ vs M between gaussian and laplacian distributions for angular spreads, σ and α with θ and ϕ fixed at 60° each, and $d = 0.2\lambda$

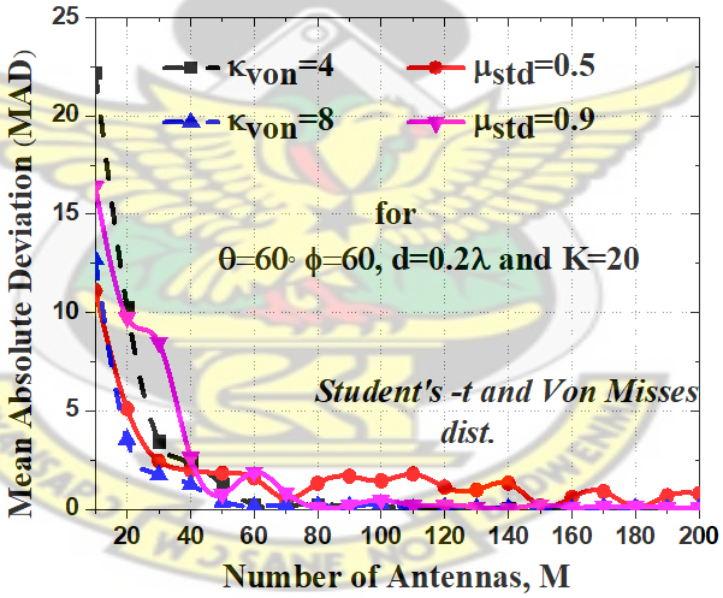

Figure 4.44: Comparing the $MAD(\mathbf{E})$ vs M between von missess and student's t-distributions for angular spreads, κ and μ with θ and ϕ fixed at 60° each, and $d = 0.2\lambda$

Computing for the Diagonal Dominance (DD)

In computing the diagonal dominance, the channel convergence deteriorates to zero as the number of antennas, M increases. However, the results demonstrates clearly the effect of varying the performance parameters on the convergence.

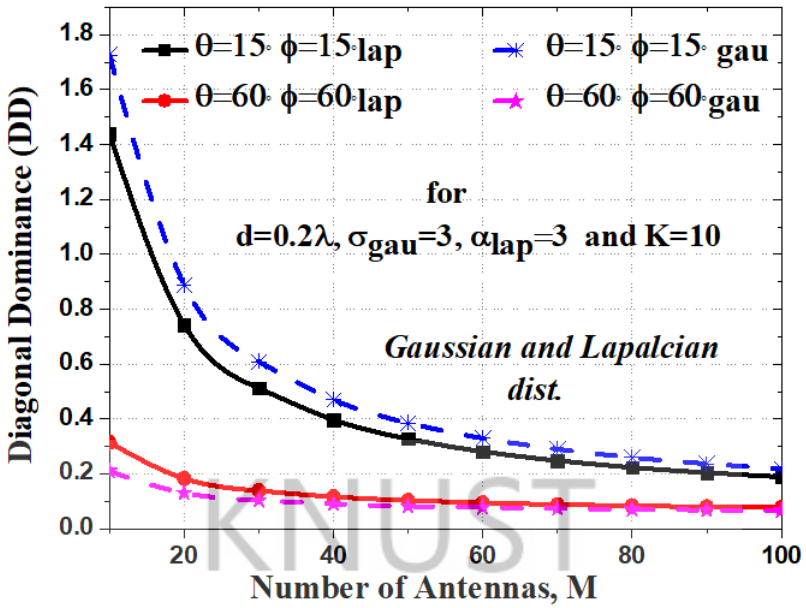

Figure 4.45: Comparing the DD vs M between gaussian and laplacian distributions with $d = 0.2\lambda, \sigma = 3, \alpha = 3$ and $K = 20$ for varying angles of θ and ϕ.

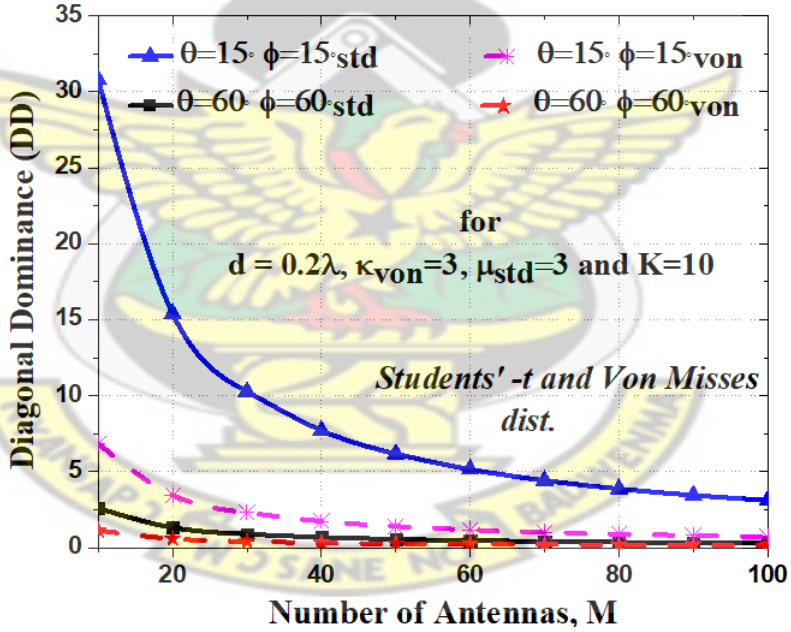

Figure 4.46: Comparing the DD vs M between von misses and student's -t distributions with $d = 0.2\lambda, \kappa = 8, \mu = 0.9$ and $K = 20$ being fixed for varying angles of θ and ϕ.

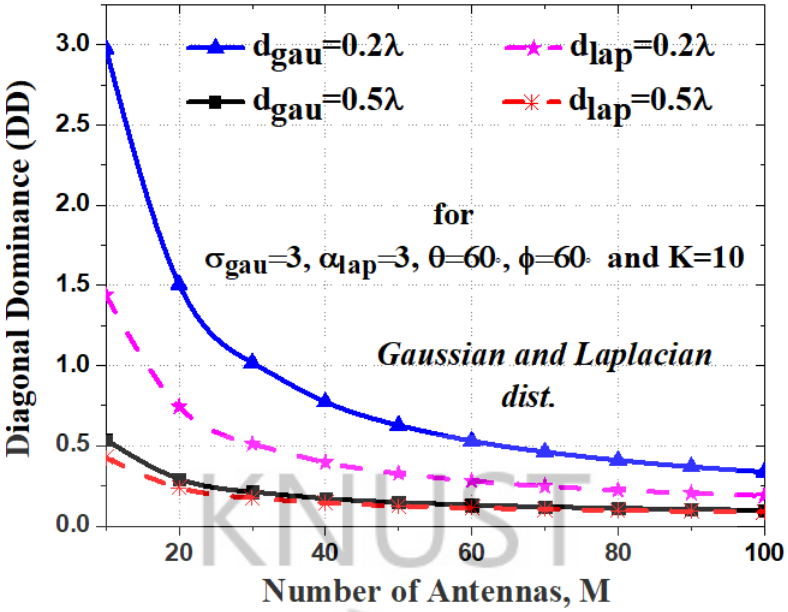

Figure 4.47: Comparing the DD vs M between gaussian and laplacian distributions for varied antenna element spacing, d with θ and ϕ fixed at 60° each, and $\sigma = 3$ and $\alpha = 3$

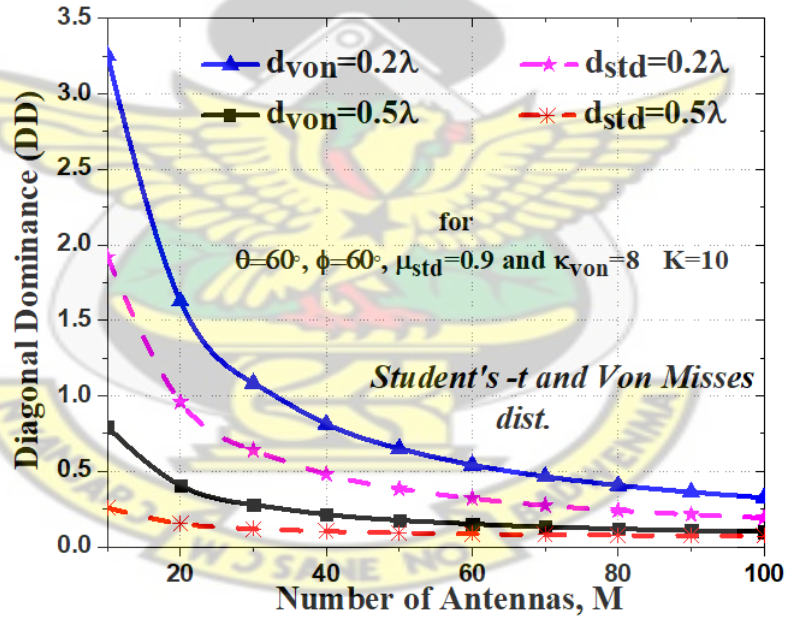

Figure 4.48: Comparing the DD vs M between von misses and student' t-distributions for varied antenna element spacing, d with θ and ϕ fixed at 60° each, and $\kappa = 8$ and $\mu = 0.9$

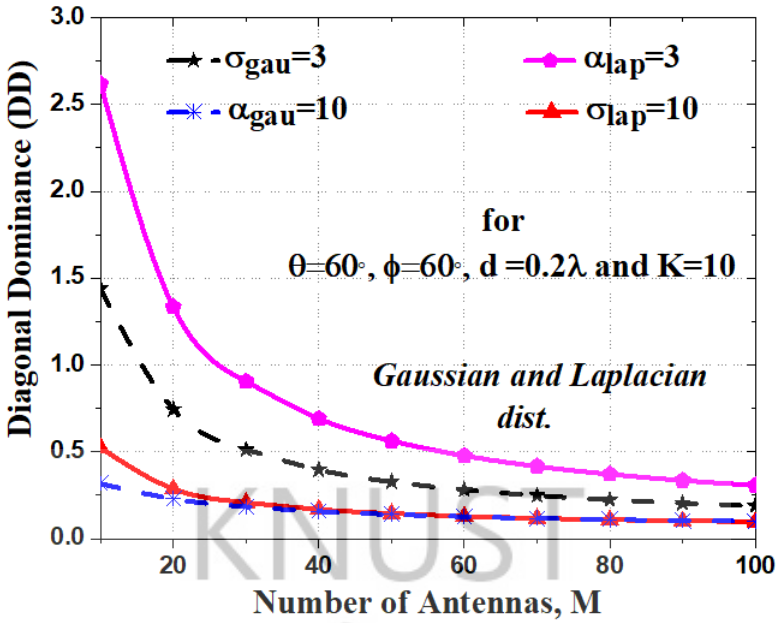

Figure 4.49: Comparing the DD vs M between gaussian and laplacian distributions for angular spreads, σ and α with θ and ϕ fixed at 60° each, and $d = 0.2\lambda$

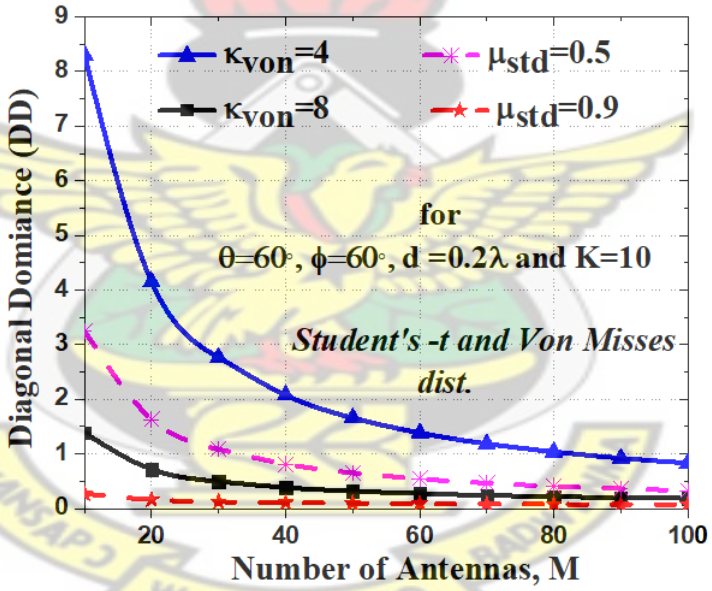

Figure 4.50: Comparing the DD vs M between von missess and student's t-distributions for angular spreads, κ and μ with θ and ϕ fixed at 60° each, and $d = 0.2\lambda$

Computing for MAD as both K and M increases

From Figures 4.51 and 4.52, results demonstrate that the channel convergence deviates from favorable propagation as the number of users, K approach the number of antennas, M. However, the convergence was better for increasing d just as similar results were realized for the case of the URA antenna topology.

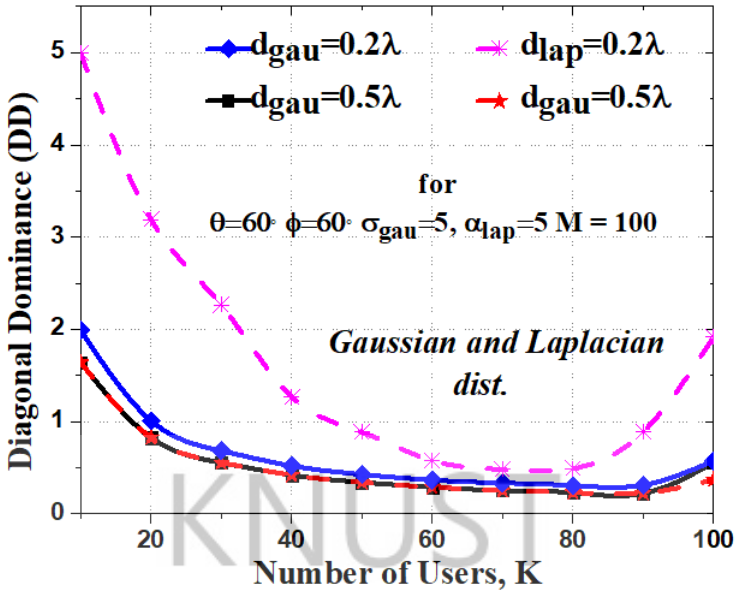

Figure 4.51: MAD vs M for K increasing with α, σ, θ and ϕ remaining constant whilst varying the distance bewteen antenna elements, d.

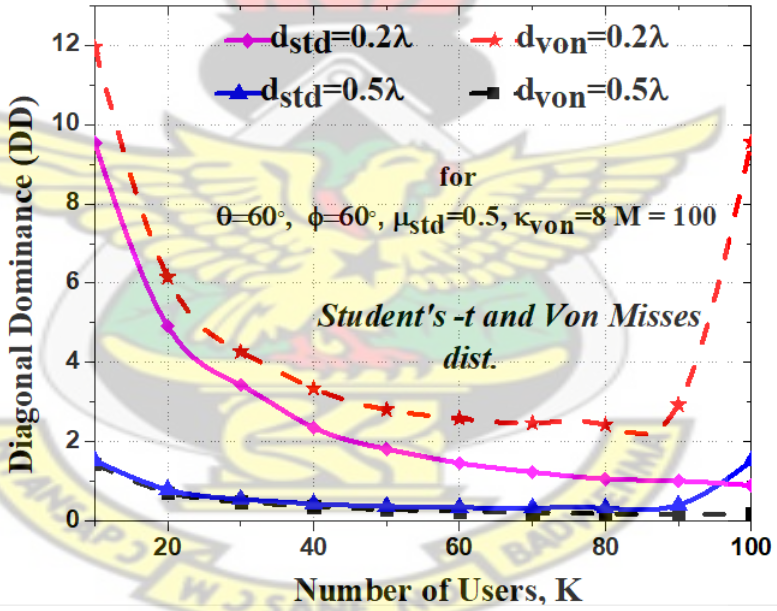

Figure 4.52: MAD vs M for K increasing with κ, μ, θ and ϕ remaining constant whilst varying the distance between antenna elements, d.

4.4 Analysis of URA antenna

From the results of the URA antenna, it can be observed that convergence rate increases as the AS and ES, antenna element spacing and the spread of the angular distributions increases, for the Gaussian and Student's -t distributions.

However, in the Von Misses and Laplacian distributions, poor convergence performances were recorded for analysis using the GBSCM. This poor performance can be attributed to the high spatial correlation coefficients registered, as the number of antenna elements increased. Therefore, increasing the AS and ES, the spacing between antenna elements, as well as the spreads of the distribution did not significantly reduce the spatial correlation thereby affecting the convergence performance.

4.5 Analysis of CA antenna

Unlike that of the URA, simulation results of the CA antenna show good convergence performance for all the various distributions used in the analysis. This can be attributed to the difference in antenna element arrangement and array topology used. Hence, relatively lower values of spatial correlation were registered for all the different distributions of arrivals used. It observed that the rate of convergence increases as both θ and ϕ increases. This is as a result of the decrease in the spatial correlation as both θ and ϕ values increases. Also, increasing the spreads of the distribution, σ, α, μ and κ reduces the spatial correlation between the antenna elements, thereby increasing the convergence rate even as the number of antennas increases.

Chapter 5

Conclusion and Recommendations

5.1 Conclusion

In this thesis, the spatial correlation (SC) of large-scale antenna array topologies (Uniform rectangular array and Cylindrical Array) was derived based on the Maximum Power of Arrival (MPA) concept. The MPA concept presents an exact and precise approach of generalizing the SC expression of antenna arrays for different angular distributions. This therefore reduces the need to generate distinct SC expressions of specific antenna array regarding different angular distributions. The Convergence was examined for both the 3D Geometry-Based Stochastic Channel Model (GBSCM) based on 3GPP and WINNER+, and the Correlation-Based Stochastic Channel Model (CBSCM) for each of the antenna arrays (URA and CA). While the Correlation-Based Stochastic Channel Model is used for theoretical analysis of wireless communication channels, the Geometry-Based Stochastic Channel Model (GBSCM) on the other hand reflects the real practical massive MIMO Channel. For this work, four different distributions of angle of arrivals were used which includes the Laplacian, Von Misses, Gaussian and Student's t-distributions. The effect of the SC on convergence were analyzed in each of the distributions as the increase in azimuth (AS) and elevation (ES) spreads of the angular distributions of arrival and antenna elements spacing were varied.

Results support existing developments that increasing the antenna element spacing reduces the correlation thereby increasing the rate at which massive MIMO systems converge to favorable propagation. Results also demonstrate that increasing the azimuth and elevation spreads of the angle of arrivals of the various distributions decreases the correlation and thereby increases the rate of conver-

gence. However, the Laplacian and Von Misses distributions showed poor performances in the geometry-based stochastic channel model.

Again, in the analysis of both the uniform rectangular array (URA) and the cylindrical array (CA), the convergence was sensitive to the different array antenna topologies regarding the 3D geometry-based stochastic channel model.

5.2 Future Work

For this thesis, two antenna array topologies were used, which includes the uniform rectangular antenna array and the cylindrical antenna array, to study the effects of the SC on convergence of massive MIMO to favorable propagation. This work can be further extended to include analysis for other antenna array topologies such as the spherical antenna array. Again, this thesis did not take into account the effects of the mutual coupling that will form between the antenna elements on the convergence of massive MIMO systems. Mutual coupling between antennas can be modeled between (ideal) dipole antenna elements. In general, mutual coupling between two antenna elements can be interpreted as the voltage produced at the terminal of one antenna element as a result of a current being induced on the other antenna element [58]. Works have demonstrated that the Mutual Coupling (MC) influences the resultant spatial correlation and system performance, especially for close inter-element antenna spacing.

To have a more precise performance characterization of the 3D massive MIMO system, the mutual coupling effect, $\mathbf{Z}$ between the transmitter and receiver antenna pairs must be considered in future work for the convergence analysis to reflect real practical performance.

5.3 Challenges

The MATLAB simulation for the generation of the channel parameters took relatively very long computational time due to the large matrix dimensions generated.

Also, the MATLAB computation for $M \geq 200$ number of antennas took relatively very long and often resulted in system crashes, as the dimensions of the matrices computed grew large.

REFERENCES

[1] Jensen, M. A. (2016, June). A history of MIMO wireless communications. In *2016 IEEE International Symposium on Antennas and Propagation (APSURSI)* (pp. 681-682). IEEE

[2] Brennan, D. G. (1959). Linear diversity combining techniques. *Proceedings of the IRE*, (6), 1075-1102.

[3] Vaughan, R. G., & Andersen, J. B. (1987). Antenna diversity in mobile communications. *IEEE Transactions on vehicular technology*, 36(4), 149-172.

[4] Jensen, M. A., & Rahmat-Samii, Y. (1994). Performance analysis of antennas for hand-held transceivers using FDTD. *IEEE Transactions on Antennas and Propagation*, 42(8), 1106-1113.

[5] Foschini, G. J. (1996). Layered space-time architecture for wireless communication in a fading environment when using multi-element antennas. *Bell labs technical journal*, 1(2), 41-59.

[6] Foschini, G. J., & Gans, M. J. (1998). On limits of wireless communications in a fading environment when using multiple antennas. *Wireless personal communications*, 6(3), 311-335

[7] Raleigh, G. G., & Cioffi, J. M. (1998). Spatio-temporal coding for wireless communication. *IEEE Transactions on communications*, 46(3), 357-366.

[8] Alamouti, S. (2000). A simple transmit diversity technique for wireless communications. *IEEE Journal on Selected Areas in Commun.,* 16(8), 2817-2821.

[9] Spencer, Q. H., Jeffs, B. D., Jensen, M. A., & Swindlehurst, A. L. (2000). Modeling the statistical time and angle of arrival characteristics of an indoor

multipath channel. *IEEE Journal on Selected areas in communications*, 18(3), 347-360

[10] Cho, Y. S., Kim, J., Yang, W. Y., & Kang, C. G. (2010). *MIMO-OFDM wireless communications with MATLAB*. John Wiley & Sons.

[11] Cho, Y., & Lee, J. H. (1999). Effect of fading correlation on the SER performance of M-ary PSK with maximal ratio combining. *IEEE communications letters*, 3(7), 199-201

[12] Loyka, S. L. (2001). Channel capacity of MIMO architecture using the exponential correlation matrix. *IEEE Communications letters*, 5(9), 369-371.

[13] Telatar, E. (1999). Capacity of multi-antenna Gaussian channels. *European transactions on telecommunications*, 10(6), 585-595.

[14] Manteuffel, D. (2009, November). MIMO antenna design challenges. In 2009 *Loughborough Antennas & Propagation Conference* (pp. 50-56). IEEE.

[15] Kammoun, A., Debbah, M., & Alouini, M. S. (2015). A generalized spatial correlation model for 3D MIMO channels based on the Fourier coefficients of power spectrums. *IEEE Transactions on Signal Processing*, 63(14), 3671-3686.

[16] Dahlman, E. (2014). IWPC evolutionary and disruptive visions towards ultra high capacity networks. *White paper version*, 1.

[17] Osseiran, A., Boccardi, F., Braun, V., Kusume, K., Marsch, P., Maternia, M., ... & Tullberg, H. (2014). Scenarios for 5G mobile and wireless communications: the vision of the METIS project. *IEEE communications magazine*, 52(5), 26-35.

[18] Agiwal, M., Roy, A., & Saxena, N. (2016). Next generation 5G wireless networks: A comprehensive survey. *IEEE Communications Surveys & Tutorials*, 18(3), 1617-1655.

[19] Andrews, J. G., Buzzi, S., Choi, W., Hanly, S. V., Lozano, A., Soong, A. C., & Zhang, J. C. (2014). What will 5G be?. *IEEE Journal on selected areas in communications*, 32(6), 1065-1082.

[20] Wang, C. X., Haider, F., Gao, X., You, X. H., Yang, Y., Yuan, D., ... & Hepsaydir, E. (2014). Cellular architecture and key technologies for 5G wireless communication networks. *IEEE communications magazine*, 52(2), 122-130.

[21] Larsson, E. G., Edfors, O., Tufvesson, F., & Marzetta, T. L. (2013). Massive MIMO for next generation wireless systems. *arXiv preprint arXiv:*1304.6690.

[22] Rusek, F., Persson, D., Lau, B. K., Larsson, E. G., Marzetta, T. L., Edfors, O., & Tufvesson, F. (2012). Scaling up MIMO: Opportunities and challenges with very large arrays. *arXiv preprint arXiv:*1201.3210.

[23] Marzetta, T. L. (2010). Noncooperative cellular wireless with unlimited numbers of base station antennas. *IEEE Transactions on Wireless Communications*, 9(11), 3590.

[24] Hosseini, K., Hoydis, J., Ten Brink, S., & Debbah, M. (2013, June). Massive MIMO and small cells: How to densify heterogeneous networks. In *ICC 2013* (pp. 5442-5447).

[25] Finn, D., Ahmadi, H., Cattoni, A. F., & DaSilva, L. A. (2015). Improved spectral efficiency through multiuser MIMO across small cells. *IEEE Transactions on Vehicular Technology*, 65(9), 7764-7768.

[26] Balanis, C. A. (2016). *Antenna theory: analysis and design*. John wiley & sons.

[27] Zheng, K., Ou, S., & Yin, X. (2014). Massive MIMO channel models: A survey. *International Journal of Antennas and Propagation*, 2014.

[28] Zhao, L., Yeung, L. K., & Wu, K. L. (2014). A coupled resonator decoupling network for two-element compact antenna arrays in mobile terminals. *IEEE Transactions on Antennas and Propagation*, 62(5), 2767-2776

[29] Yong, S. K., & Thompson, J. S. (2003, October). A 3-dimensional spatial fading correlation model for electromagnetic vector sensors. In *6th International SYmposium on Antennas, Propagation and EM Theory, 2003. Proceedi* 2003 (pp. 843-846). IEEE.

[30] Masouros, C., Sellathurai, M., & Ratnarajah, T. (2013). Large-scale MIMO transmitters in fixed physical spaces: The effect of transmit correlation and mutual coupling. *IEEE Transactions on Communications*, 61(7), 2794-2804.

[31] Couillet, R., & Debbah, M. (2011). *Random matrix methods for wireless communications*. Cambridge University Press.

[32] Ngo, H. Q., Larsson, E. G., & Marzetta, T. L. (2014, September). Aspects of favorable propagation in massive MIMO. In *2014 22nd European Signal Processing Conference (EUSIPCO)* (pp. 76-80). IEEE.

[33] Wu, X., Beaulieu, N. C., & Liu, D. (2017). On favorable propagation in massive MIMO systems and different antenna configurations. *IEEE Access*, 5, 5578-5593.

[34] Hochwald, B. M., Marzetta, T. L., & Tarokh, V. (2004). Multiple-antenna channel hardening and its implications for rate feedback and scheduling. *IEEE transactions on Information Theory*, 50(9), 1893-1909.

[35] Smith, P. J., Neil, C., Shafi, M., & Dmochowski, P. A. (2014, June). On the convergence of massive MIMO systems. In

2014 IEEE International Conference on Communications (ICC) (pp. 5191-5196). IEEE.

[36] Kammoun, A., Debbah, M., & Alouini, M. S. (2015). 3D massive MIMO systems: Modeling and performance analysis. *IEEE Transactions on wireless communications*, 14(12), 6926-6939.

[37] Sharma, S. K. (2012). Characterization and modeling of MIMO wireless channels based on correlation tensor. *Computers & Mathematics with Applications, 64(2)*, 89-101.

[38] Hoydis, J., Ten Brink, S., & Debbah, M. (2013). Massive MIMO in the UL/DL of cellular networks: How many antennas do we need?.

[39] Yin, H., Gesbert, D., Filippou, M., & Liu, Y. (2012). A coordinated approach to channel estimation in large-scale multiple-antenna systems. *arXiv preprint arXiv:*1203.5924.

[40] Clerckx, B., Craeye, C., Vanhoenacker-Janvier, D., & Oestges, C. (2007). Impact of Antenna Coupling on 2×2 MIMO Communications. *IEEE Transactions on Vehicular Technology*, 56(3), 1009-1018.

[41] Masouros, C., Chen, J., Tong, K., Sellathurai, M., & Ratnarajah, T. (2013, July). Towards massive-MIMO transmitters: On the effects of deploying increasing antennas in fixed physical space. In *2013 Future Network & Mobile Summit* (pp. 1-10). IEEE.

[42] 3GPP. 3GPP TR 36.873 V12.0.0 , *Study on 3D channel model for LTE*,

[43] Payami, S., & Tufvesson, F. (2012, March). Channel measurements and analysis for very large array systems at 2.6 GHz. In *2012 6th European Conference on Antennas and Propagation (EUCAP)* (pp. 433-437). IEEE.

[44] Gao, X., Tufvesson, F., Edfors, O., & Rusek, F. (2012, November). Measured propagation characteristics for very-large MIMO at 2.6 GHz. In *ACSCC* (pp. 295-299).

[45] Gao, X., Tufvesson, F., Edfors, O., & Rusek, F. (2012). Channel behavior for very-large MIMO systems-initial characterization. In *COST IC1004*, 2012.

[46] Wang, C. X., & Wu, S. Massive MIMO channel measurements and modeling: Advances and challenges. *IEEE Wireless Commun.*

[47] Wu, S., Wang, C. X., Haas, H., Alwakeel, M. M., & Ai, B. (2014). A non-stationary wideband channel model for massive MIMO communication systems. *IEEE transactions on wireless communications*, 14(3), 1434-1446.

[48] Ghazal, A., Wang, C. X., Haas, H., Beach, M., Lu, X., Yuan, D., & Ge, X. (2012, May). A non-stationary MIMO channel model for high-speed train communication systems. In *2012 IEEE 75th Vehicular Technology Conference (VTC Spring)* (pp. 1-5). IEEE.

[49] Aulin, T. (1979). A modified model for the fading signal at a mobile radio channel. *IEEE Transactions on Vehicular Technology, 28(3)*, 182-203.

[50] Kalliola, K., Laitinen, H., Vainikainen, P., Toeltsch, M., Laurila, J., & Bonek, E. (2003). 3-D double-directional radio channel characterization for urban macrocellular applications. *IEEE Transactions on Antennas and Propagation, 51*(11), 3122-3133.

[51] Meinila, J., Kyosti, P., Hentila, L., Jamsa, T., Suikkanen, E., Kunnari, E., & Narandzic, M. (2010). D5. 3: WINNER+ final channel models. *Wireless World Initiative New Radio WINNER.*

[52] Zhong, Z., Yin, X., Li, X., & Li, X. (2013, September). Extension of ITU IMT-advanced channel models for elevation domains and line-of-sight scenar-

ios. In *2013 IEEE 78th Vehicular Technology Conference (VTC Fall)* (pp. 1-5). IEEE

[53] Danae, C. (2013). Technical specification group radio access network. Technical report, Technical report, Spreading and Modulation, http://www. 3gpp. org.

[54] Nam, Y. H., Ng, B. L., Sayana, K., Li, Y., Zhang, J., Kim, Y., & Lee, J. (2013). Full-dimension MIMO (FD-MIMO) for next generation cellular technology. *IEEE Communications Magazine, 51*(6), 172-179.

[55] IST-WINNER (2006). *WINNER 11 interim channel models.*

[56] Muirhead, R. J. (2009). *Aspects of multivariate statistical theory* (Vol. 197). John Wiley & Sons.

[57] Masouros, C., Chen, J., Tong, K., Sellathurai, M., & Ratnarajah, T. (2013, July). Towards massive-MIMO transmitters: On the effects of deploying increasing antennas in fixed physical space. In *2013 Future Network & Mobile Summit* (pp. 1-10). IEEE.

[58] Clerckx, B., Craeye, C., Vanhoenacker-Janvier, D., & Oestges, C. (2007). Impact of Antenna Coupling on 2×2 MIMO Communications. *IEEE Transactions on Vehicular Technology*, 56(3), 1009-1018.

[59] Thiele, L., Wirth, T., BÃ¶rner, K., Olbrich, M., Jungnickel, V., Rumold, J., & Fritze, S. (2009, February). Modeling of 3D field patterns of downtilted antennas and their impact on cellular systems. In *International ITG Workshop on Smart Antennas (WSA 2009).*

[60] Kuchar, A., Rossi, J. P., & Bonek, E. (2000). Directional macro-cell channel characterization from urban measurements. *IEEE Transactions on Antennas and Propagation, 48*(2), 137-146.

[61] Mohajer, M., & Safavi-Naeini, S. (2009, March). MIMO antenna optimization using method of moments analysis. In *2009 IEEE International Workshop on Antenna Technology* (pp. 1-4). IEEE.

[62] Zhou, J., Sasaki, S., Muramatsu, S., Kikuchi, H., & Onozato, Y. (2003, December). Spatial correlation for a circular antenna array and its applications in wireless communication. In *GLOBECOM'03. IEEE Global Telecommunications Conference (IEEE Cat. No. 03CH37* (Vol. 2, pp. 1108-1113). IEEE.

[63] Andersen, J. B., & Pedersen, K. I. (2002). Angle-of-arrival statistics for low resolution antennas. *IEEE Transactions on Antennas and Propagation, 50*(3), 391-395.

[64] Yong, S. K., & Thompson, J. S. (2005). Three-dimensional spatial fading correlation models for compact MIMO receivers. *IEEE Transactions on Wireless Communications, 4*(6), 2856-2869.

[65] Forenza, A., Love, D. J., & Heath, R. W. (2007). Simplified spatial correlation models for clustered MIMO channels with different array configurations. *IEEE Transactions on Vehicular Technology, 56*(4), 1924-1934.

[66] Pedersen, K. I., Mogensen, P. E., & Fleury, B. H. (1997). Power azimuth spectrum in outdoor environments. *Electronics Letters, 33*(18), 1583-1584.

[67] Tsai, J. A., Buehrer, R. M., & Woerner, B. D. (2002). Spatial fading correlation function of circular antenna arrays with Laplacian energy distribution. *IEEE Communications Letters, 6*(5), 178-180.

[68] Queiroz, W. J., Madeiro, F., Lopes, W. T. A., & Alencar, M. S. (2011). Spatial correlation for DoA characterization using Von Mises, Cosine, and Gaussian distributions. *International Journal of Antennas and Propagation*, 2011.

[69] Ren, J., & Vaughan, R. G. (2009, September). Spaced antenna design in directional scenarios using the von mises distribution. In *2009 IEEE 70th Vehicular Technology Conference Fall* (pp. 1-5). IEEE.

[70] Teal, P. D., Abhayapala, T. D., & Kennedy, R. A. (2002). Spatial correlation for general distributions of scatterers. *IEEE signal processing letters, 9*(10), 305-308.

[71] Ying, D., Vook, F. W., Thomas, T. A., Love, D. J., & Ghosh, A. (2014, June). Kronecker product correlation model and limited feedback codebook design in a 3D channel model. In *2014 IEEE International Conference on Communications (ICC)* (pp. 5865-5870). IEEE.

[72] Neil, C. T., Shafi, M., Smith, P. J., & Dmochowski, P. A. (2015, June). On the impact of antenna topologies for massive MIMO systems. In *2015 IEEE International Conference on Communications (ICC)* (pp. 2030-2035). IEEE.

[73] Kammoun, A., Debbah, M., & Alouini, M. S. (2016, July). Spatial correlation characterization of a uniform circular array in 3D MIMO systems. In *2016 IEEE 17th International Workshop on Signal Processing Advances in Wireless Com* (pp. 1-6). IEEE.